Quaternary Research (2023), **111**, 148–165
doi:10.1017/qua.2022.39

Research Article

Implications for catchment weathering, provenance, and climatic records from a late Pleistocene to present sedimentary sequence in Gujarat, India

Kamlesh Kumar[a]*, Anupam Sharma[a], Pradeep Srivastava[b] and Biswajeet Thakur[a]

[a]Birbal Sahni Institute of Palaeosciences 53, University Road, Lucknow, 226007, India and [b]Indian Institute of Technology, Roorkee, Uttarakhand, 247667, India

Abstract

To ascertain weathering, provenance, and paleoclimate of the last ca. 29 ka in mainland Gujarat, western India, a sedimentary profile of ~7.5 m was measured, described, and sampled at Pratappura and a multiproxy analysis was conducted. To determine weathering, silty-sand and sandy-silt facies were analyzed, and log Na_2O/K_2O versus log SiO_2/Al_2O_3 was plotted, which shows clustering in the quartz arenite and sub-litharenite categories, indicating low to moderate weathering. The chemical index of alteration (CIA) is 55–74, and was plotted versus the index of chemical variability (ICV) of 1.50, with samples clustered mainly between subalkali basalt and picrite, indicating the dominance of a mafic component. While depleted chondrite normalized light rare earth element (REE) (La/Yb <1) levels suggest the prevalence of a mafic source in the catchment, identical chondrite normalized REE patterns indicate that sediments were well homogenized. Using multiple proxies, the measured profile was subdivided into five paleoclimatic zones. Zone-I (29–18 ka) exhibits decreasing moisture, C_{org}, χ_{lf}, Al_2O_3, TiO_2, and Fe_2O_3 trends, while higher values of CO_3^{-2} and $\delta^{13}C$ indicate a change from a warm-humid to semiarid climate. Zone-II (18–11 ka) shows signs of the beginning of aridity ca. 18 ka during the Last Glacial Maximum (LGM). Several proxies in zone-III show wetter climatic conditions from the early Holocene (ca. 11–4 ka) due to the onset of the SW monsoon, with the trend continuing in zone-IV (4–2 ka). In zone-V, the climate appears to have been similar to the modern conditions in the area from 2 ka–present.

Keywords: Geochemistry, Paleoclimate, Late Pleistocene, Provenance, Multiproxy analysis, REE, Magnetic susceptibility, Phytoliths

(Received 7 October 2021; accepted 10 July 2022)

INTRODUCTION

Numerous researchers have examined fluvial deposits and their relationship with geomorphological features, depositional environments, and paleoclimatic records (e.g., Cant and Walker, 1978; Bridge, 1985; Bristow, 1996). Conventional wisdom holds that past hydrological conditions (climate) can be deduced from the coupled effects of morphological and sedimentological parameters on fluvial sequences. Understanding fluvial responses to climate variability is crucial to paleoclimate reconstructions (Schumm, 1993; Knox, 1995). West-central India has seen extensive research into the geomorphological, sedimentological, structural, depositional, and chronological aspects of Quaternary fluvial deposits, particularly in the Mahi-Narmada-Sabarmati river basins (Maurya et al., 1995, 1997, 2000; Merh and Chamyal 1997; Raj et al., 1998; Jain and Tandon, 2003; Jain et al., 2004; Bhandari et al., 2005; Juyal et al., 2006; Prasad et al., 2007; Singh et al., 2007; Laskar et al., 2010). According to these studies, the fluvial sediments of the Mahi-Narmada-Sabarmati river basins are stratigraphically correlatable, and were deposited under comparable climatic and tectonic conditions.

Three surfaces—alluvial plain (-S1), ravinal (-S2) and valley-fill (-S3)—have been recognized and used to separate the fluvial deposits of Mahi-Narmada-Sabarmati river basins (Juyal et al., 2000; 2003; 2006; Maurya et al., 2000). The fluvial deposits may be a sign of past environmental changes associated with changing monsoon circulation patterns. According to Jain and Tandon (2003), the fluvial systems in western India responded to global climate changes such that fluctuations in monsoon intensity modulated relative changes in discharge and sediment supply. Furthermore, Tandon et al. (1997) and Juyal et al. (2000, 2004, 2006) linked variation in the dynamics of the Indian summer monsoon (ISM) to changes in fluvial deposits. According to Juyal et al. (2006), conditions in the mainland Gujarat region were wetter during the early phase of Marine Isotope Stage 2 (MIS-2) than they are at present. However, river discharges into the Bay of Bengal and the Arabian Sea decreased during the Last Glacial Maximum (LGM; ca. 20 ka) because of a weak monsoon. Due to rising aridity, drainage in the Thar Desert was severely affected, and fluvial processes were essentially inactive. The monsoon intensified ca. 15–13 ka, affecting the drainage systems of the Indian subcontinent. This period was marked by an abrupt and large increase in the monsoon intensity followed by the early Holocene humid phase ca. 9–6 ka (Bhattacharya et al., 2017). Additionally, the S-1 and S-3 surfaces of the Mahi River

*Corresponding author email address: kamleshk2508@gmail.com

Cite this article: Kumar K, Sharma A, Srivastava P, Thakur B (2023). Implications for catchment weathering, provenance, and climatic records from a late Pleistocene to present sedimentary sequence in Gujarat, India. *Quaternary Research* **111**, 148–165. https://doi.org/10.1017/qua.2022.39

© University of Washington. Published by Cambridge University Press, 2022

https://doi.org/10.1017/qua.2022.39 Published online by Cambridge University Press

show an age difference of ca. 5 ka, from 10 ka to 5 ka (i.e., between Early and the mid-Holocene). Together, enhanced monsoonal precipitation and tectonic uplift in the early Holocene caused a 5-ka chronological gap in the geological records (Maurya et al., 1997, 2000). Additionally, there are few studies using laboratory-based data focusing on the texture, mineralogy, and geochemistry of the sediments, making it difficult to accurately estimate the intensity of the climate regime responsible for sediment transport, as well as determining depositional environments, degree of weathering, and provenance of sediments, all of which have important climatic implications.

Therefore, we examined sediment deposits in the Dhadhar River basin, located between the Narmada and Mahi river catchments of Gujarat in western India. We discovered a natural embankment/levee sedimentary deposit located between the Mahi and Narmada river basins along the Khakariya Nala, a tributary of the Dhadhar River that drains into Pratappura Lake, that we termed the 'Pratappura profile.' The Pratappura profile is a ~7.5 m sedimentary sequence that allows us to fill in missing information due to the chronological gap in the geological record as currently known in the area.

We utilized a multiproxy approach to analyzing the Pratappura profile using grain size, geochemistry, χ_{lf}, $\delta^{13}C$, and phytoliths to analyze textural and geochemical characteristics of this deposit. Our goals were to: 1) characterize textural and mineralogical characteristics of the sediments, 2) determine the extent of weathering of the sediments, 3) determine the provenance of the sediment, and 4) integrate the data to better understand the climate history of this area for the past ca. 29 ka (MIS-2 to present).

Study area

The Pratappura section is located ~25 km (22°29.002 N; 73° 23.522 E) northeast of Vadodara City (Fig. 1a). A natural embankment that we called the Pratappura section is located next to Pavagarh Hill (Fig. 1a, c). The Dhadhar River is eventually formed by the joining of first and second order streams which also drain into Pratappura Lake. The subhumid Narmada basin in the south and the semiarid Mahi basin in the north are linked by the Dhadhar River.

The geology of the research region consists of Precambrian basement overlain by Jurassic, Cretaceous, Tertiary, and Quaternary rocks in different areas (Biswas, 1987). Rock formations that are found along the two major lineaments, the Narmada and the Cambay rift systems (Fig. 1b), show uplift and subsidence along the Mesozoic and Cenozoic tectonic features that left traces on the majority of mainland Gujarat (Biswas, 1987). Cretaceous fault-controlled sedimentary basins show evidence of tectonic activity associated with these two significant (Narmada and Cambay rift) fracture trends. In contrast, modern distribution and outcrop patterns demonstrate an E–W-trending fault control. Tertiary rocks were deposited in tectonic basins bounded by N–S and E–W-trending faults. Quaternary deposits are separated from older rocks in the area by the N–S-trending eastern Cambay Basin fault that continues across the mainland. The terrain, which often exhibits progressive stepping down from south to north along E–W faults and from east to west along N–S faults, reflects underlying structure (Fig. 1b).

The region experiences variable rainfall (2000 mm in the south and 300 mm in the north; Fig. 1a) and our research area falls within arid and semiarid climate zones. Although temperatures peak up to 47–48°C during the summer, the daily mean maximum and minimum temperatures are ~40°C and 25°C, respectively. A climatology graph of the study area includes mean annual precipitation (MAP) and mean annual temperature (MAT) (Fig. 1d).

The lithology of the Pratappura section is composed of sand, silt, and clay. Silty sand and tough, massive calcrete make up the bottom 1.8 m of the profile (Fig. 1c). The calcrete is overlain by a massive, >1 m-thick sandy horizon with no visible sedimentary structures. A 1.2-m-thick layer of silty clay lies above the sandy horizon which is then overlain by >1 m beds of alternating sand and clay units. The top of the section is composed of ~ 2.5-m-thick friable and homogenous sand with a few calcrete nodules. A total of 104 sediment samples were collected at 5-cm intervals from the base of the section to 4.5 m, and at 20-cm intervals from 4.5 m to 7.5 m due to less lithological variation. Four samples were taken from sandy layers for optically stimulated luminescence (OSL) analysis to determine the section's precise chronology.

METHODS

Optically stimulated luminescence (OSL) dating

For optically stimulated luminescence (OSL) chronology, four sandy-to-silty samples (Fig. 2, Table 1) were dated by the Wadia Institute of Himalayan Geology, Dehradun (WIHG). The fundamental presumption behind OSL dating is that sand loses its stored luminescence when exposed to sunlight during erosion and transit, a process known as 'zeroing.' Due to radioactive exposure from ambient U, Th, K, and gamma radiation, the same sediment resumes accumulating luminescence after sedimentation and burial. The laboratory equivalent of the luminescence thus accumulated is called equivalent dose (ED). By dividing the ED by the dose rate, the age of the sediment can be determined. Due to turbulence, zeroing can be difficult in fluvially produced sediments, and fresh feldspar contamination can frequently obscure the OSL signal. These issues are resolved by 1) utilizing a minimum age model (MAM) to treat data with overdispersion (OD) of less than 20% and the mean ages for the data with a larger OD (Galbraith et al., 1999), and 2) observing the infrared stimulated luminescence (IRSL) signal for feldspar, which should have fewer than 150 counts.

The samples were chemically treated using H_2O_2 and HCl in the laboratory to remove organic matter and carbonate coatings. Subsequently, the dried sediment was sieved to 125–150 μm. A density separation technique using sodium polytungstate (density = 2.59 gm/cc) was applied for quartz and feldspar separation. First, HF was used to remove the alpha-affected skin from the separated quartz grains, and then HCl was used to dissolve the fluoride crystals. The quartz grains were then mounted on 9.8 mm stainless steel discs after being washed, dried, and cleaned. For measuring the ED, a Riso TL/OSL-20 system equipped with arrays of blue LEDs and infrared LEDs as a source for stimulation at 125°C for 40 s was employed. For each sample, 35 aliquots were used. Photons were counted for paleodose estimation using a combination of Schott BG-39 and Hoya U-340 optical filters in front of an EMI 9235 QA photomultiplier tube. A 5-point single aliquot regeneration (SAR) technique was employed for the measurement, with a preheat of 220°C/10 s and a cut heat of 160°C (Murray and Wintle, 2000). IRSL measurements on natural samples were used to track feldspar contamination. Using photon

https://doi.org/10.1017/qua.2022.39 Published online by Cambridge University Press

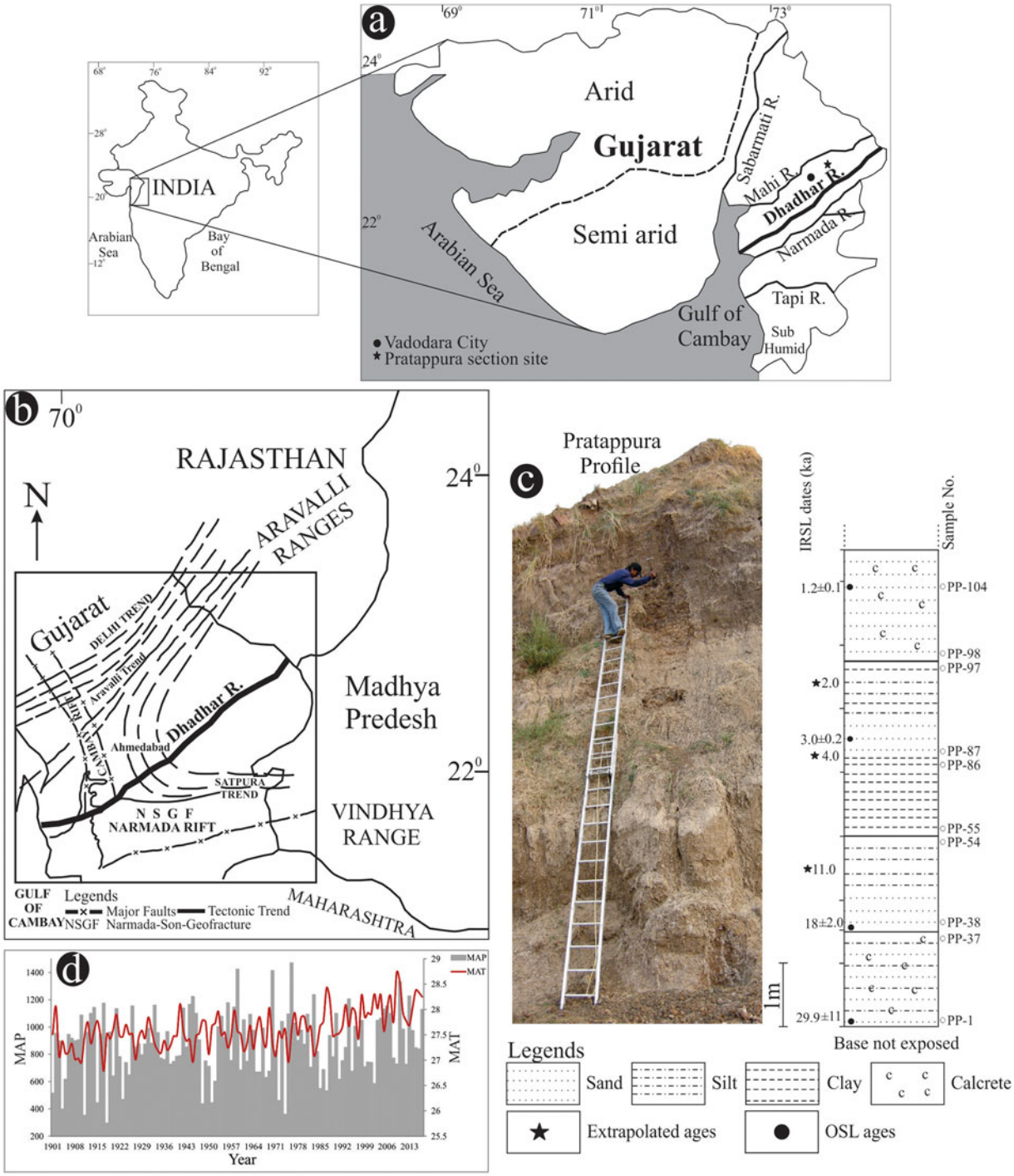

Figure 1. Geographic setting, tectonic trends, climate, lithology, photo, and graphic measured stratigraphic section of the study area. Map of India at top left indicates where (a) regional and local study areas are located in Gujarat. (b) Regional tectonic setting showing prominent structural trends, faults, and rifts. (c) Field photograph and associated graphic stratigraphic section showing lithology of the profile, where samples were taken for optically stimulated luminescence (OSL) analysis, and infrared stimulated luminescence (IRSL) and extrapolated ages. (d) Climatology graph of the study area indicating mean annual temperature (MAT) in °C and mean annual precipitation (MAP) in mm per year.

counts from the shine-down curves of the initial 5 channels (1 channel = 0.16 s), the paleodose for 30–35 discs was determined. U, Th, and K concentrations were measured using X-ray fluorescence (XRF) and inductively coupled plasma mass spectrometry (ICP-MS) for dose rate calculations. These samples were considered to have a moisture content of 10 ± 5% and a cosmic dose rate of 150 ± 30 μGyr^{-1} (Prescott and Stephan, 1982).

Digital elevation model (DEM)

With a resolution of 90 m, a digital elevation model (DEM) was produced using data from the Shuttle Radar Topographic Mission (SRTM; https://srtm.csi.cgiar.org) as inputs for Spatial Analyst in ArcGIS 10.3 (Fig. 3). Based on symmetry, channels and stream lineaments were recovered from the DEM to create

https://doi.org/10.1017/qua.2022.39 Published online by Cambridge University Press

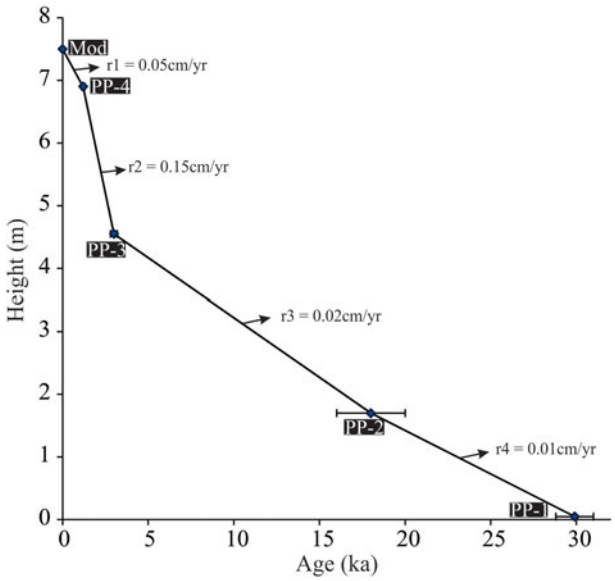

Figure 2. Age-depth model showing optically stimulated luminescence (OSL) dates and sedimentation rates (r) derived from the Pratappura section. Mod: modern; see Figure 1c for sample locations.

a drainage map. The ROSE diagram was prepared in RockWare 16 (Wells, 1999), a useful tool for visually representing two-dimensional orientation and other data (Potter and Pettijohn, 1963; Wells 1999; Sanderson and Peacock, 2020), and the azimuths were calculated for all the escarpments in the study area using ArcGIS 10.3. The azimuths of the channel and stream lineaments were also then calculated using ArcGIS 10.3 (ESRI, 2011). Using the Rose module in RockWare, the azimuths were then plotted as a rose diagram to organize the lineament association according to their direction of propagation. The resulting rose diagram shows how lineaments repeat at regular intervals (Moore et al., 1991; Reddy, 1991).

Textural (grain-size) and loss-on-ignition (LOI) analyses

For grain-size analysis, 35 sediment samples were chosen from the measured profile (Supplementary Table S1). Following the methods of Jackson (1956) and Kunze (1965), 10 g of bulk, air-dried samples were treated with CH_3COONa, H_2O_2, $NaHCO_3$, and $Na_2S_2O_4$ to remove carbonate, organic carbon, salts, and iron-manganese oxide coatings on the sediment grains. A 53-µm sieve was used to separate the sand fraction from silt and clay. After that, distilled water was added to the silt and clay fraction and transferred into a 1-L cylinder to separate the silt and clay fraction by the pipette method (Tanner and Jackson, 1948; Day, 1965). A ternary diagram was then created that plotted the percentages of sand, silt, and clay in the samples.

A total of 104 sediment samples were evaluated for moisture, organic carbon (C_{org}), and inorganic carbon (CO_3^{-2}) percentages. Five g of 75-µm powder samples were cooked in quartz crucibles at 110°C, 550°C, and 950°C, and weight loss was measured to quantify moisture, C_{org}, and CO_3^{-2} (weight loss at 950°C is multiplied by a factor of 1.36 to covert weight loss from CO_2 to CO_3), in the samples, respectively (Dean, 1974; Bengtsson and Enell, 1986).

Magnetic susceptibility (χ_{lf}) analysis

Magnetic susceptibility (χ_{lf}) is a concentration-dependent parameter of ferrimagnetic and paramagnetic content in the sediment. The χ_{lf} is used as a proxy to infer climatic variations (Maher and Thompson, 1992; Evans and Heller, 1994; Sangode and Mazari, 2007; Phartiyal et al., 2009). Higher values of χ_{lf} imply a close relationship between erosional processes and increasing concentration of detrital input from the catchment (Williamson et al., 1999). Samples were analyzed using low field mass-specific susceptibility (χ_{lf}). For these analyses, ~10-g samples were (Supplementary Table S2) was taken in non-magnetic sample holders and analyzed using a MS-2 Bartington susceptibility meter at WIHG, Dehradun.

Stable carbon isotope analysis

Stable carbon isotope analysis was performed on 48 sediment samples (Supplementary Table S3). Samples were air-dried, powdered, and then 1.5 g per sample was repeatedly treated with 5% HCl and heated on a water bath for 2 hours to dissolve the carbonates. Acid-treated samples were then rinsed in Milli-Q water and centrifuged at 3000 round per minute (rpm) to remove the acid and soluble salts. After complete neutralization, the samples were dried in a hot air oven at 50°C. The treated dry samples were then powdered, weighed, and properly packed into tin capsules. The samples were analyzed in a mass spectrometer (FLASH-EA 1112 Series Thermo made) at the Indian Institute of Tropical Meteorology (IITM), Pune. Isotopic results are given using delta (δ) notation using the international standard Vienna PeeDee Belemnite (VPDB; Coplen, 1994). Measurement error was ± 0.1‰ based on repeated analysis of a laboratory standard.

Bulk and clay mineral X-ray diffraction (XRD) analyses

For bulk mineralogical studies, six samples were selected from the profile. The air-dried samples were crushed to 75 µm and

Table 1. Optically stimulated luminescence (OSL) chronology of Pratappura profile. Least represents the minimum age. The wide spread in the paleodose data suggests inhomogeneous bleaching of geological luminescence signal, which prompted us to use the least 20% of the paleodoses of final age calculation.

Lab No.	Sample number	Height (m)	U (ppm)	Th (ppm)	K (%)	Dose rate (Gy/ka)	Paleodose (Gy)		Age (ka)	
							Mean	Least	Mean	Least
LD-795	PP-4	6.90	1.3	7.8	1.1	2.0 ± 0.1	4 ± 1	2.5 ± 0.2	2.0 ± 0.2	1.2 ± 0.1
LD-887	PP-3	4.55	1.31	10	1.04	2.0 ± 0.1	10 ± 2	6 ± 0.3	5 ± 1	3.0 ± 0.2
LD-888	PP-2	1.70	4.16	12	1.16	2.8 ± 0.2	74 ± 15	52 ± 3	26 ± 6	18.0 ± 2.0
LD-794	PP-1	0.05	1.4	8.1	1.1	2.1 ± 0.1	67 ± 4	62 ± 1	32.3 ± 2.2	29.9 ± 1.1

https://doi.org/10.1017/qua.2022.39 Published online by Cambridge University Press

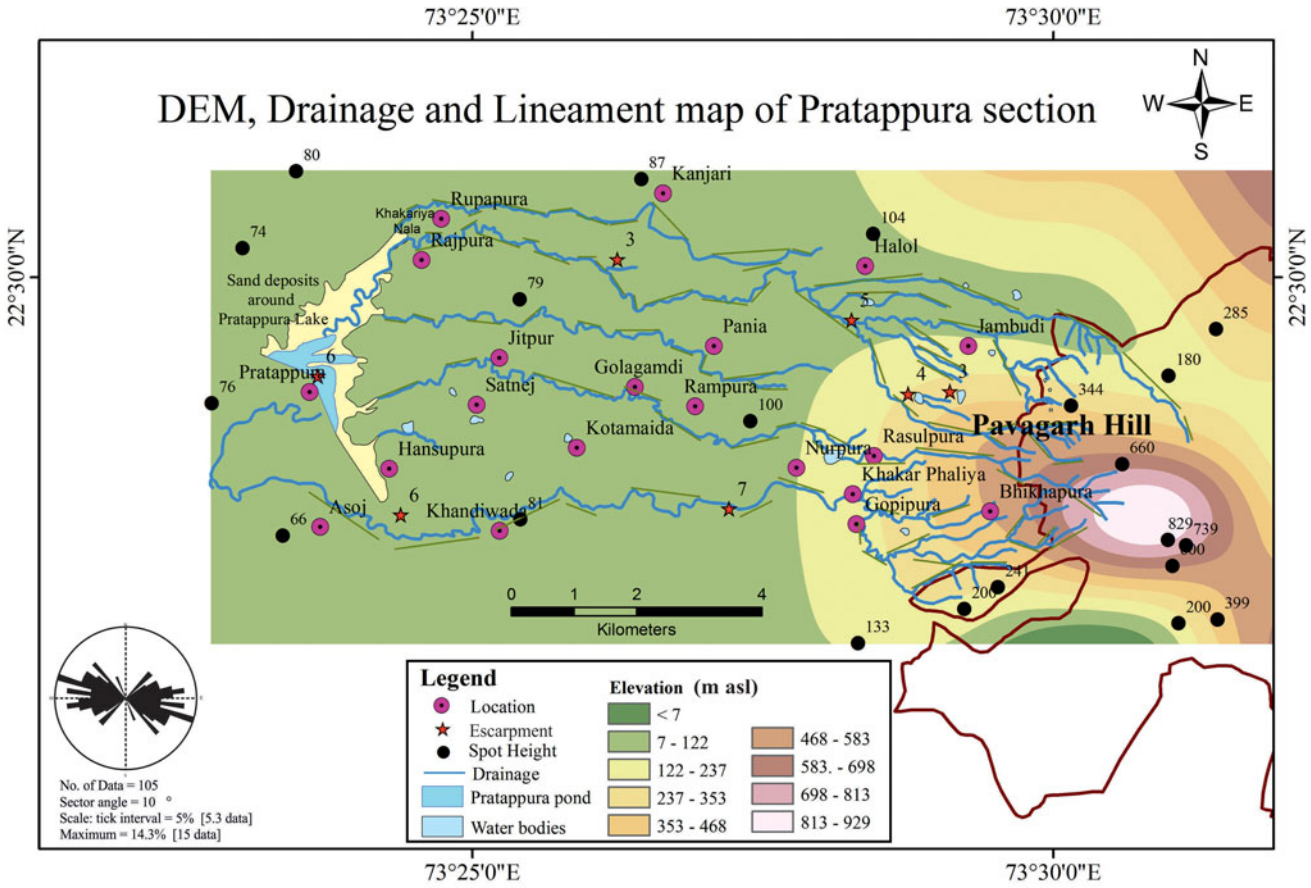

Figure 3. Digital elevation model (DEM), subsurface lineament, escarpment, and rose diagram for the Pratappura profile area, showing the structurally controlled drainage pattern.

analyzed using an XPERT-PRO diffractometer system with continuous scanning at 25°C (2θ of 4.0–79.9). For clay mineralogy, eight samples were selected from the profile. The clay fraction (<2 μm) was separated, and oriented slides were prepared using a standard smear technique (Tanner and Jackson, 1948; Day, 1965). The clay slides were analyzed (2θ of 4.0–40.0) using a XPERT-PRO diffractometer at WIHG. The identification of clay minerals was done by glycolation, then heating samples at 250°C and 300°C. Mineral identification was done using X'pert high score software (https://www.malvernpanalytical.com) and the ICDD pdf 4 mineral database (Gates-Rector and Blanton, 2019).

Geochemical analysis

For bulk geochemical analysis, 16 sediment samples were chosen from the entire profile (Table 2). The bulk samples were initially homogenized using the coning and quartering method, and ~25 g sample was crushed to 75 μm using a Retsch (PM 100 CM) disc mill. For major oxide analysis, 6 g of powdered sample and 4 g of boric acid were mixed, and pressed pellets were prepared for XRF analysis (Stork et al., 1987; Saini et al., 2000; Khanna et al., 2009). The pellets were analyzed for major and minor oxides using a standard wavelength-dispersive X-ray fluorescence spectrometer (WD-XRF) technique on a sequential XRF spectrometer (Siemens SRS-30 0 0) at WIHG, Dehradun. Several international sediment sample standards (GXR-2, SO-1, GSS-1, SCO-1, SGR-1, MAG-1, and GSD-9) were used to check the precision and accuracy of the sample preparation and instrumental performance. The accuracy and the precision of measurement were better than 2–5% and <2%, respectively. For a few trace elements including rare earth element (REE) analysis, samples were digested in a mixture of super-pure acids ($HF + HNO_3 + HClO_4$) using the 'B-solution' method (Shapiro and Brannock, 1962) in Teflon™ crucibles. All samples were analyzed by ICP-MS (PerkinElmer, Elan-DRCe) at WIHG, Dehradun. Several USGS international (MAG-1, SGR-1, SCo-1) and in-house (WIHG, Dehradun) standards were used for instrument calibration. The precision for ICP-MS analyses obtained was ≤5%.

Chemical index of alteration (CIA) calculations were carried out by using the molar proportion of Al_2O_3, CaO*, Na_2O and K_2O. CaO* was taken in silicate form only (Nesbitt and Young, 1989), and calculated by the method proposed by McLennan (1993) because we had no direct method available to distinguish and quantify the amount of CaO belonging to the silicate and non-silicate fractions. The CIA was calculated as:

$$CIA = Al_2O_3/(Al_2O_3 + CaO* + Na_2O + K_2O)*100 \quad (Eq.1)$$

and in a generalized A (Al_2O_3)–CN (CaO* + Na_2O)–K (K_2O) triangular plot, the average upper continental crust (UCC) composition is ~50 (CIA = ~50).

https://doi.org/10.1017/qua.2022.39 Published online by Cambridge University Press

https://doi.org/10.1017/qua.2022.39 Published online by Cambridge University Press

Table 2. Major, trace, and rare earth element (REE) compositions of samples from the Pratappura profile with calculated chemical index of alteration (CIA) and index of chemical variability (ICV) values; ppm: parts per million.

Sample Number	PP-1	PP-6	PP-10	PP-15	PP-21	PP-29	PP-38	PP-47	PP-58	PP-63	PP-73	PP-82	PP-86	PP-92	PP-100	PP-104
Major Oxides (%)																
SiO_2	57.2	56.0	50.6	56.5	57.2	54.2	73.6	70.9	72.1	65.9	68.5	65.7	69.3	64.8	71.9	71.1
Al_2O_3	11.7	11.4	9.0	10.3	12.4	7.6	8.7	10.0	8.8	10.5	8.7	9.7	8.9	10.1	8.6	8.5
TiO_2	1.69	1.53	1.10	1.32	0.77	0.92	0.74	0.65	0.88	0.78	1.05	0.59	1.29	1.29	0.91	0.90
Fe_2O_3	7.85	7.38	6.13	6.49	5.11	4.34	4.45	5.85	4.50	6.47	4.66	5.58	5.01	5.52	5.44	5.34
MnO	0.10	0.10	0.09	0.09	0.08	0.06	0.06	0.08	0.07	0.09	0.09	0.08	0.10	0.14	0.10	0.09
MgO	2.12	2.13	2.63	2.04	1.50	1.26	1.09	1.54	0.89	1.33	0.85	1.41	0.89	1.03	1.07	1.05
CaO	3.36	5.81	11.69	7.82	2.78	12.07	0.69	1.16	0.64	0.90	1.03	1.89	1.13	2.00	1.02	1.03
Na_2O	0.79	0.85	0.55	0.74	2.02	0.60	0.74	0.67	0.74	0.73	0.78	0.66	0.97	0.97	0.69	0.67
K_2O	1.14	1.24	1.01	1.14	2.80	0.92	1.05	1.30	0.99	1.24	0.91	1.29	1.27	1.26	1.34	1.23
P_2O_5	0.10	0.09	0.04	0.08	0.19	0.06	0.04	0.07	0.02	0.09	0.02	0.04	0.08	0.09	0.08	0.08
Trace Element (ppm)																
Ba	351	365	351	339	550	307	395	345	380	360	354	356	328	424	370	368
Co	27.5	25.0	21.3	21.8	15.4	15.6	18.8	16.8	21.1	19.5	23.3	17.7	18.2	23.7	20.1	19.2
Cr	73.7	157	133	151	160	132	190	169	225	144	194	82.6	98.3	149	156	152
Ni	63.0	56.5	38.2	52.9	29.7	40.1	51.6	37.1	55.4	37.5	52.9	36.3	39.9	47.1	33.0	32.0
Rb	59.2	126	50.2	121	128	106	152	62.6	181	73.2	74.3	62.6	64.3	71.3	63.6	61.0
Sr	410	483	562	476	191	335	158	126	159	128	145	119	117	161	113	111
Y	20.4	20.6	19.7	21.3	48.0	19.1	19.7	19.0	22.8	19.9	22.6	18.6	17.3	21.7	19.0	18.0
Zr	127	122	140	118	112	82.3	86.0	96.0	95.9	119	139	102	111	113	124	121
CIA	74.8	72.7	74.9	73.1	55.3	71.2	70.8	72.9	71.9	73.1	70.3	72.5	65.4	68.1	69.2	66.3
ICV	1.45	1.67	2.58	1.91	1.21	2.66	1.01	1.12	0.99	1.10	1.08	1.18	1.19	1.21	1.23	1.22
REE (ppm)																
La			27.1					25.7		27.5		24.7			26.4	
Ce			52.7					52.2		53.5		45.8			54.3	
Nd			24.9					23.9		25.1		21.1			24.5	
Sm			5.30					5.03		5.34		4.53			5.23	
Eu			1.05					0.91		1.03		0.87			0.92	
Gd			3.62					3.29		3.44		3.15			3.54	
Dy			3.71					3.48		3.65		3.33			3.51	
Er			1.95					1.89		1.92		1.81			1.85	
Yb			1.82					1.81		1.86		1.75			1.80	
(La/Sm)N			2.80					2.80		2.82		2.98			2.76	
(Gd/Yb)N			1.60					1.46		1.49		1.44			1.58	
(La/Yb)N			8.82					8.43		8.76		8.36			8.71	
(Eu/Eu*)N			0.74					0.70		0.74		0.71			0.67	

The index of chemical variability (ICV) was also calculated to understand the index of recycling and compositional maturity in sediments (Cox et al. 1995; Armstrong-Altrin, 2015), where

$$ICV = (Fe_2O_3 + K_2O + Na_2O + CaO + MgO + MnO + TiO_2)/Al_2O_3 \quad (Eq.2)$$

and an ICV < 1 indicates sediment recycling and that the sediment is highly mature, whereas ICV > 1 shows a first cycle of sediment deposition, and that the sediment is immature in nature.

Phytolith studies

Phytoliths are microscopic opaline silica bodies present in almost all plants, and their major function is to provide mechanical support to the plant. In the grasses, phytoliths are very distinct and their morphology is easily distinguishable between summer and winter grasses. After the decay of plants, phytoliths remain in the soil and sediment as a relic of an earlier ecosystem (paleovegetation; Fredlund and Tieszen, 1994).

For phytolith analysis, 5 g of sediment sample (Supplementary Table S4) was kept in 10% sodium hexametaphosphate (Calgon™ solution) overnight, and suspended clay was siphoned out. The samples were subsequently treated with 10% HCl and heated in a sand bath for 10–20 minutes for carbonate removal. The organic content was removed by heating 30% H_2O_2 in a sand bath for 20–30 minutes. The remaining residue was washed twice with distilled water. Phytolith extraction was done by adding the residue to a heavy liquid solution of cadmium iodide (CdI_2) and potassium iodide (KI) with a specific gravity of 2.3 that was centrifuged at 1000 rpm for 5 minutes. The lighter fraction containing phytoliths were then washed, dried, and weighed. Dried phytoliths were mounted on slides using Canada balsam. A few slides were also mounted in immersion oil to view 3-D images of phytoliths. The phytoliths were identified at 100× magnification using a Leitz LABORLUX-D light microscope and a minimum of 300 counts were taken and classified according to Twiss et al. (1969) and Mulholland and Rapp (1992).

RESULTS

Chronology

Four sediment samples for OSL dating were taken at various heights from the profile (see Figure 1c for sample locations). The samples produced a typical shine-down curve for quartz. The shine-down curve, growth curve, and cumulative frequency curve of the sample LD-795 are shown in Supplementary Figure S1. Supplementary Figure S2 displays the radial plots and OD values for all four samples. Table 1 provides information on ED, dosimetry and ages. The sedimentation rates from an age-depth model created using Microsoft Excel were used to derive the extrapolated ages (Fig. 2).

Grain size and LOI

In the sediment textural study (Fig. 4; Supplementary Table S1), the percentage distribution of sand, silt, and clay in the sedimentary succession is shown. All samples plotted in the silty-sand and sandy-silt region of the ternary plot, as shown in Supplementary Figure S3. In the profile, the percentage of sand ranges from 17–81% (average = 47%), that of silt from 18–79% (average = 49%), and that of clay from 0.9–4.7% (average = 2.94%). In zone-I (0–1.7 m), the percentages of the sand fraction varies from 17–50%, the silt fraction varies from 48–78% and the clay fraction varies from 2–4%. In zone-II (1.7–2.7 m), the percentages of sand range from 46–60%, silt from 36–50%, and clay from 2.8–3.3%. In zone III (2.7–4.20 m), silt and clay fractions rise slightly, and the clay fraction declines somewhat. Overall, sand > silt > clay in zones I and II, while in zone-III silt is more dominant. In zone IV (4.20–5.3 m), the sand and silt fractions are the main components rather than the clay fractions. The sand fraction rises even higher and the clay fraction falls in zone V (5.3–7.5 m).

The % moisture, C_{org}, and CO_3^{-2} concentrations of the sediment samples were estimated using LOI analysis (Fig. 4, Supplementary Table S2). Zone-I has a moisture content of 2% to 7%; a C_{org} content from 1.3% to 3.0%; and a CO_3^{-2} concentration of 4% to 19%. Zone-II sediments have moisture contents that range from 3.6% to 4.4%, a C_{org} content from 1.3% to 2.4%, and a CO_3^{-2} concentration of 1.4% to 4%, whereas zone-III sediments have slightly higher moisture contents of 2.8% to 6%, C_{org} of 1.3% to 3.8%, and a CO_3^{-2} concentration of 1.9% to 15%. Zone-IV shows no discernible change in the moisture and C_{org} values as compared to zone-III, whereas the CO_3^{-2} shows an increased value. In zone-V, % moisture and C_{org} values are roughly equal, and the CO_3^{-2} fraction varies between 1% and 15%.

Bulk and clay mineralogy

Six samples covering all lithologic units in Pratappura section were examined using XRD for bulk mineralogical studies (Fig. 5a). The most prevalent minerals in the sampled profile are quartz, plagioclase, and calcite. Zone-I has calcite peaks, indicating significant Ca accumulation from prolonged exposure. Zone-II contains less calcite and more quartz, mica, and pyroxene. In zone-III, there are calcite peaks that are smaller in the upper part of the zone, but the mica peak is still discernible.

Clay mineralogy was determined from eight sediment samples from the Pratappura profile (Figure 5b). Smectite, kaolinite, illite, and chlorite are present in the entire profile. Chlorite dominates over smectite in the bottom part of the profile (zone-I), whereas illite dominates in the middle part of the profile (zone II). Kaolinite/smectite predominates over other clay mineral associations in the profile from zone III to the top, however, a little amount of illite is also present in the upper part of the profile.

Magnetic susceptibility

The χ_{lf} values determined from the Pratappura profile vary from 2.08×10^{-8} m^3kg^{-1} to 21.33×10^{-8} m^3kg^{-1} (Fig. 4). At the base, ca. 29.9 ka, the highest χ_{lf} values ($21–22 \times 10^{-8}$ m^3kg^{-1}) were observed (zone-I). In the middle zones (zone II and III), the χ_{lf} does not vary much, and ranges from 2×10^{-8} m^3kg^{-1} to 3×10^{-8} m^3kg^{-1}; in the upper section (zone IV and V), the χ_{lf} ranges from 2×10^{-8} m^3kg^{-1} to 7×10^{-8} m^3kg^{-1}.

Geochemistry

Figure 6 and Table 2 depict the geochemical data as it is distributed within the sedimentary profile from Pratappura. The major oxides found in the section are SiO_2 (50–74%), Al_2O_3 (7–12%), TiO_2 (0–2%), Fe_2O_3 (4–8%), MnO (0.05–0.2%), MgO (0.5–2.7%), CaO (0.5–12%), Na_2O (0.5–2%), K_2O (1–2%) and P_2O_5 (0.015–0.2%).

https://doi.org/10.1017/qua.2022.39 Published online by Cambridge University Press

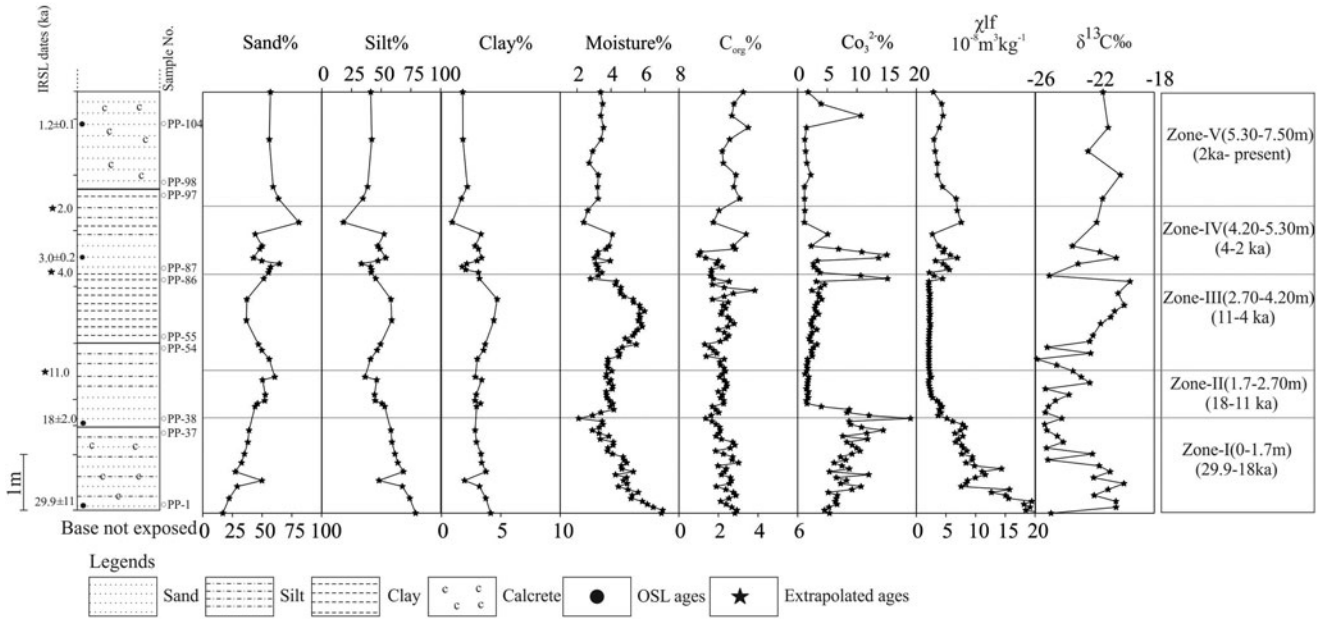

Figure 4. Pratappura profile variations with depth in sediment texture (sand, silt, and clay percentage), loss-on-ignition measurements (moisture, organic and carbonate carbon percentages), mass-specific magnetic susceptibility (χ_{lf}), and stable carbon isotopes ($\delta^{13}C$).

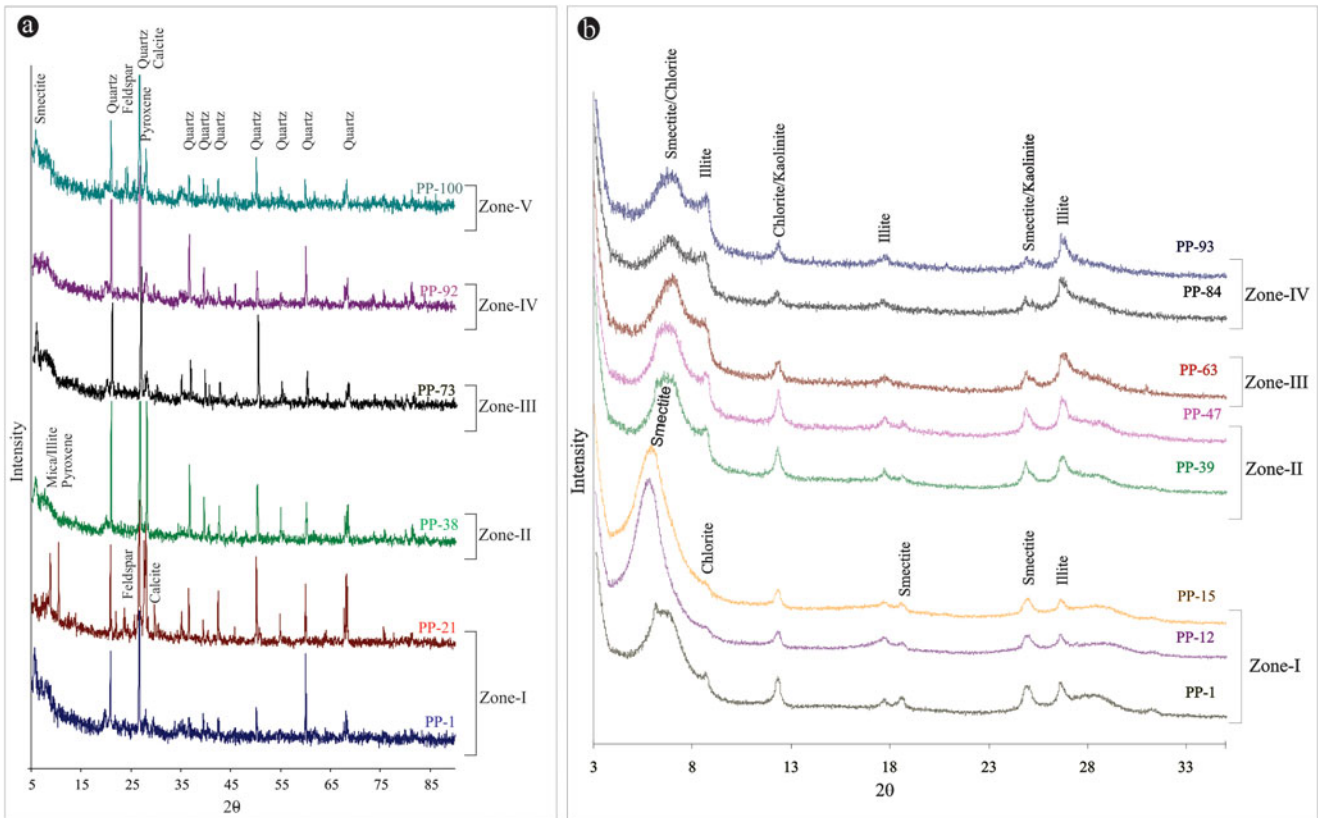

Figure 5. (a) Bulk powder X-ray diffraction (XRD) spectra and (b) clay mineral assemblage in selected Pratappura profile (PP) samples from each zone.

Variation in the sand fraction indicates changes in SiO_2 in the profile and major oxide chemistry correlates with grain size. It is evident that SiO_2 and CaO exhibit significant variation, with ranges of 50% to 75% and 0.5% to 12%, respectively. The other elements also vary, although only to a limited extent. Significant differences exist in the distribution of major oxides in the zones we defined in the profile (Fig. 6). Figure 7 shows correlation trends for the geochemical data. SiO_2 and Al_2O_3 exhibit essentially opposite fluctuation trends and are negatively correlated ($r = -0.38$). Na_2O ($r = 0.61$), MgO ($r = 0.46$), P_2O_5 ($r = 0.74$) and Fe_2O_3 ($r = 0.67$) virtually

https://doi.org/10.1017/qua.2022.39 Published online by Cambridge University Press

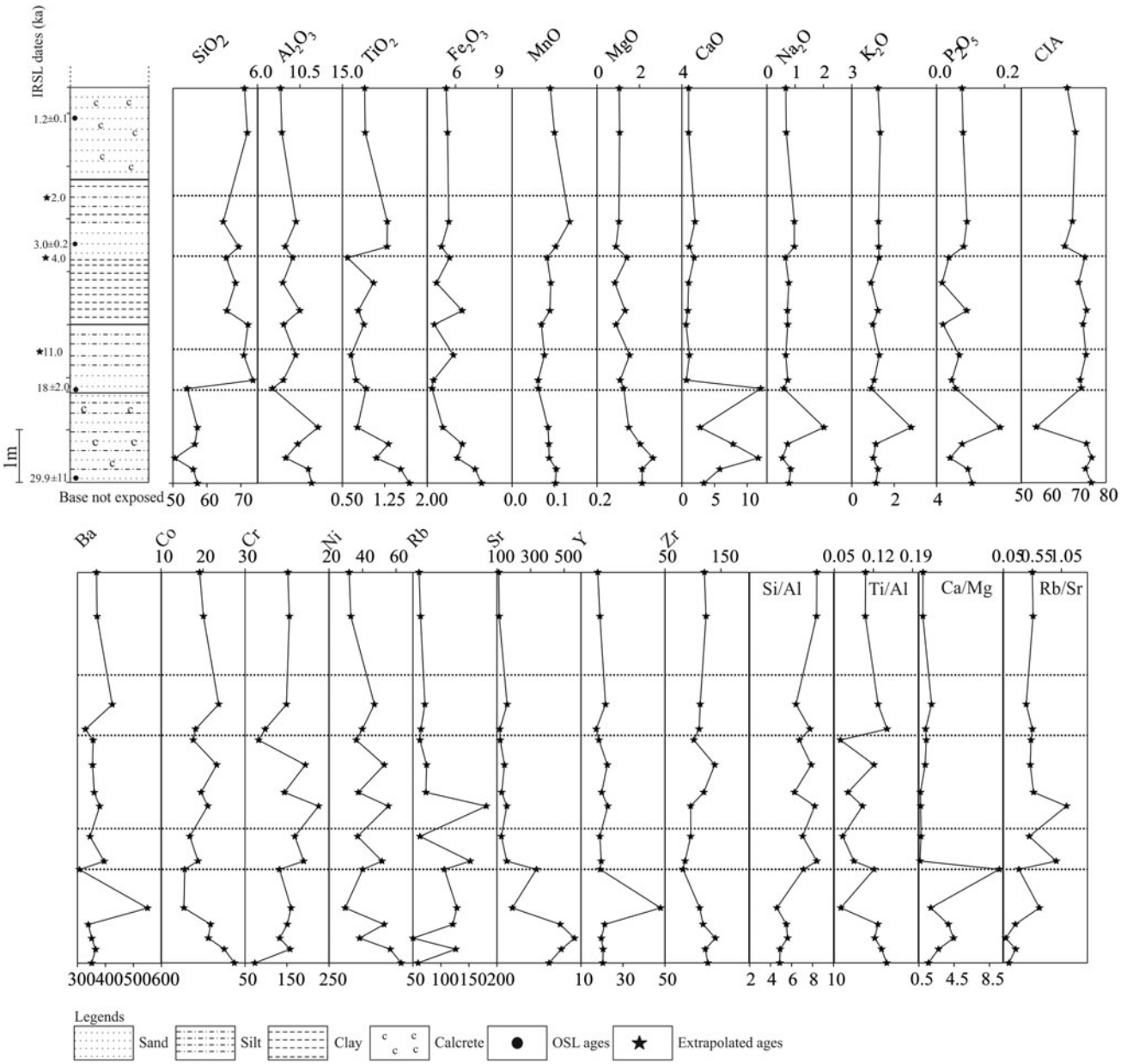

Figure 6. Variations with depth in the Pratappura profile in percentage of major oxides, trace elements in parts per million (ppm), and elemental ratios (Table 2) in selected Pratappura profile samples from each zone.

mirror the Al_2O_3 trend. The trends for CaO and Sr are also comparable (r = 0.82). The trends for Fe_2O_3, MgO, and MnO also follow one other, and TiO_2, Co, and Ni exhibit similar behavior (Table 3). The similarity between Fe_2O_3 and TiO_2 variation is interesting to note (r = 0.60). Zone-II (18 ka) has the greatest CaO/MgO value, which has a positive correlation (r = 0.65) with MgO (Table 3). Alkali feldspar control is indicated by a positive correlation between the immobile Ba and the mobile K_2O (r = 0.86). Biotite control is indicated by the Rb/Sr <1 ratio. The chondrite normalized REE patterns of a few selected samples (Table 2) are identical to the UCC. The fractionation of light REE is substantially larger (La/Sm = 2.76–2.98 versus Gd/Yb = 1.44–1.59, and variable Eu/Eu* = 0.67–0.74) than that of heavy REE (Table 2). Even while the REE pattern is the same across samples, this does not always mean that the sediments came from the same source or were homogenized in the same way.

Stable carbon isotopes ($\delta^{13}C$)

Selected samples from the complete Pratappura profile (Supplementary Table S3) were examined to determine values of $\delta^{13}C_{org}$, and to determine the trend of $\delta^{13}C$. Values of $\delta^{13}C$ vary from −25.90‰ to −19.64‰, and an average have a value of −22.68‰. The $\delta^{13}C$ value ranges from −22.09‰ to −20.04‰ in the lower part of zone-I (0–0.8 m), whereas it ranges from −25.90‰ to −22.17‰ in the upper part of zone-I (0.8–1.7 m) and zone-II. The lower and upper portions of zone-III exhibit greater negative $\delta^{13}C$ values i.e., −25.21‰ and −25.07‰

https://doi.org/10.1017/qua.2022.39 Published online by Cambridge University Press

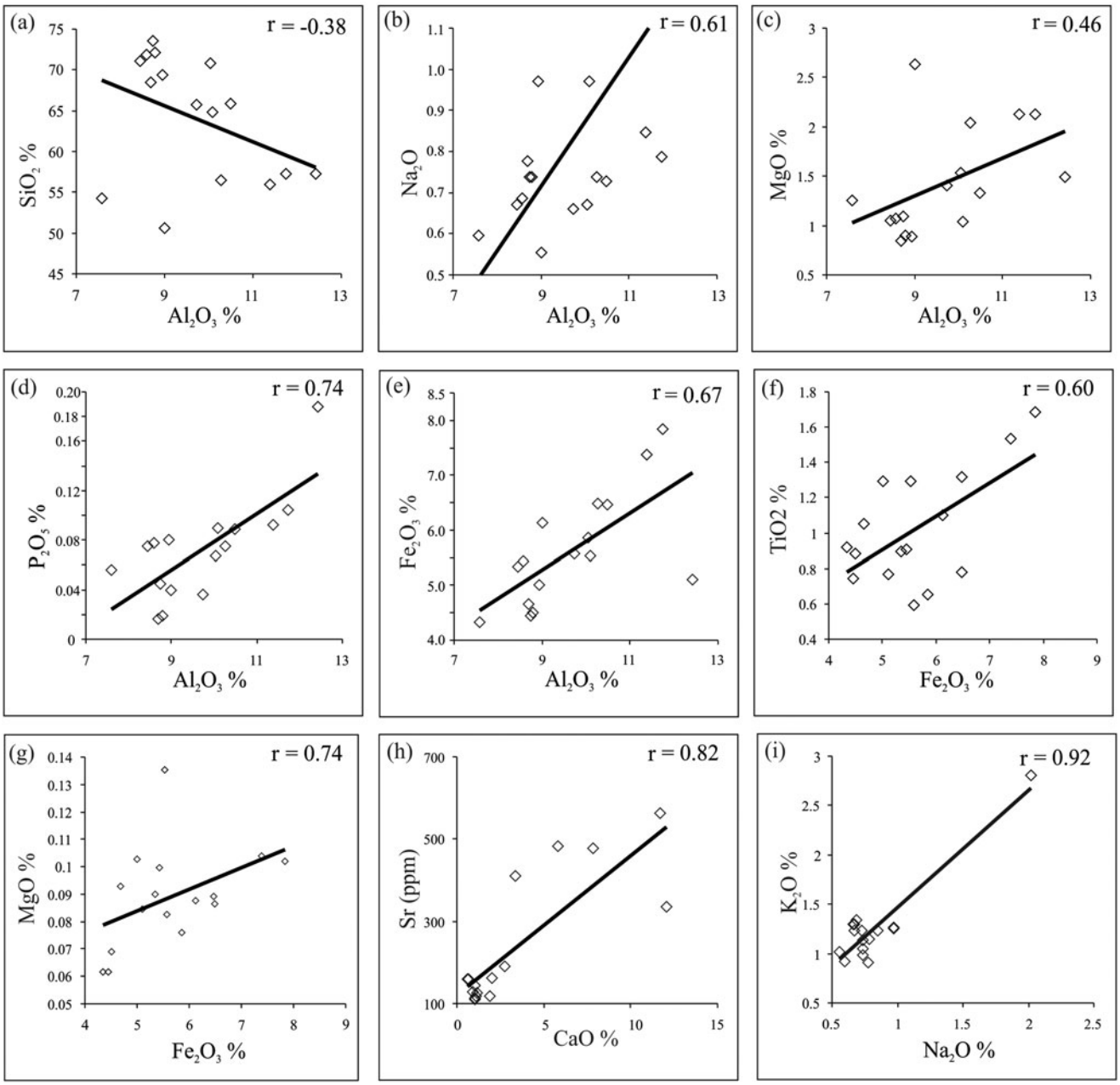

Figure 7. Binary plots showing relations among different major oxides and trace elements for Pratappura samples (Table 2).

respectively, while the central portion has slightly higher (less negative) values. the $\delta^{13}C$ values in zone-IV range from −21.88‰ to −20.28‰, except 5.07 m from the base, where they are more negative. The $\delta^{13}C$ values in the uppermost zone (zone-V) range from −22.47‰ to −21.10‰. The profile's overall $\delta^{13}C_{org}$ trend together with other proxy records can be seen in Figure 4.

Phytolith results

Phytolith remnants in the Pratappura profile are plentiful in zone-I, but most are fragmented and difficult to classify into anyone one morphotype. The predominant phytolith morphotypes in zones -II and -III (1.7 m to 4.2 m in the profile) are bulliform, which range from absent to 42% (average = 27%), rondels, which range from absent to 37% (average = 16%), trapezoid, which range from 0 to 33% (average = 15%), and rods, which range from absent to 19% (average = 8.5%). Prevalence of other phytolith morphotypes is low (Fig. 8). These phytolith morphotypes are unique to the grass families Pooideae and Fenestucoideae. While saddle, cross, and dumbbell forms are present in a few samples from the upper part of the section, globular and rough globular cells found in the upper part of the section (zones -IV and -V) range from absent to 13% (average = 4.8%) and absent to 12% (average = 2.8%), respectively. These phytolith morphotypes fall within the Panicoideae and Chloredoideae subfamilies. Very few charcoal occurrences in zone-IV and the lower portion of zone-V point to a drop in surface runoff.

https://doi.org/10.1017/qua.2022.39 Published online by Cambridge University Press

https://doi.org/10.1017/qua.2022.39 Published online by Cambridge University Press

Table 3. Correlation coefficient matrix for major and trace elements of Pratappura section; n = 16; statistical significance of numbers in bold and underlined = 99%; numbers in bold statistical significance = 95%.

	SiO_2	Al_2O_3	TiO_2	Fe_2O_3	MnO	MgO	CaO	Na_2O	K_2O	P_2O_5	Ba	Co	Cr	Ni	Rb	Sr	Y	Zr
SiO_2	1																	
Al_2O_3	−0.39	1.00																
TiO_2	−0.46	0.33	1.00															
Fe_2O_3	−0.47	**0.67**	**0.61**	1.00														
MnO	−0.09	0.35	**0.60**	0.44	1.00													
MgO	**−0.79**	0.48	0.42	**0.74**	0.05	1.00												
CaO	**−0.86**	−0.10	0.28	0.17	−0.17	**0.65**	1.00											
Na_2O	−0.16	**0.62**	−0.03	−0.09	0.17	−0.07	−0.19	1.00										
K_2O	−0.14	**0.63**	−0.21	0.00	0.10	0.03	−0.18	**0.92**	1.00									
P_2O_5	−0.32	**0.74**	0.18	0.33	0.33	0.20	−0.04	**0.80**	**0.85**	1.00								
Ba	−0.02	**0.54**	−0.20	−0.14	0.14	−0.09	−0.28	**0.88**	**0.86**	**0.67**	1.00							
Co	−0.19	0.29	**0.80**	**0.62**	**0.57**	0.34	0.00	−0.23	−0.39	−0.11	−0.17	1.00						
Cr	0.39	−0.24	−0.32	−0.47	−0.32	−0.36	−0.23	0.06	−0.04	−0.25	0.26	−0.07	1.00					
Ni	−0.12	0.17	**0.65**	0.33	0.10	0.19	0.04	−0.23	−0.48	−0.27	−0.25	**0.77**	0.13	1.00				
Rb	0.05	0.05	−0.09	−0.31	−0.47	−0.14	0.00	0.26	0.11	−0.01	0.31	−0.08	**0.63**	0.39	1.00			
Sr	**−0.86**	0.26	**0.61**	**0.57**	0.03	**0.88**	**0.83**	−0.14	−0.18	0.05	−0.21	0.44	−0.22	0.42	0.07	1.00		
Y	−0.26	**0.57**	−0.16	−0.13	−0.04	0.04	−0.04	**0.93**	**0.89**	**0.70**	**0.89**	−0.26	0.20	−0.22	0.35	−0.03	1.00	
Zr	−0.28	0.25	0.47	**0.50**	**0.57**	0.38	0.07	0.01	0.00	0.10	0.01	**0.59**	−0.15	0.07	**−0.50**	0.33	0.03	1.00

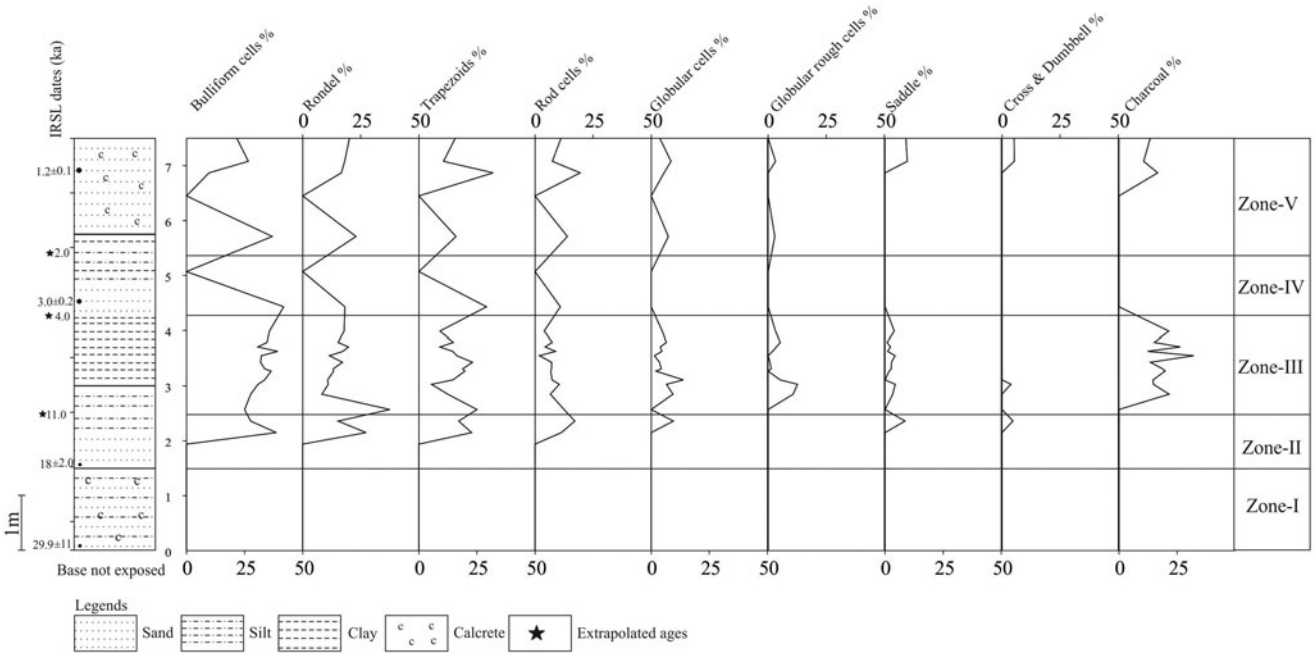

Figure 8. Depth variations in phytolith morphotypes (in %), and comparison with stable carbon isotopes ($\delta^{13}C$) in different zones from the Pratappura profile. IRSL: infrared stimulated luminescence; black dots indicate samples taken for optically stimulated luminescence (OSL) analysis.

DISCUSSION

Numerous prior research studies used catchment geomorphology, lithology, provenance, weathering, erosion, and digenetic changes in sediments to examine environmental and climatic variations during the past 125 ka (e.g., Khadkikar et al., 2000; Laskar et al., 2010; Sharma et al., 2013 and references therein) from Gujarat, Western India. Additionally, Andrews et al. (1998) and Juyal et al. (2006) reconstructed the paleoclimate of the Thar Desert, and western India, respectively. To determine the catchment weathering intensity, provenance, and paleoclimate for the past 30 ka, our investigation on the Pratappura profile in mainland Gujarat, western India, employed a multiproxy approach including inorganic geochemistry, phytoliths, and stable carbon isotope ($\delta^{13}C$) and textural analyses.

Samples from several zones revealed noticeable variation in mineralogy and geochemistry (Fig. 6). The variation in mineral composition, especially in zones -II and -III, indicated the presence of specific mineral phases, such as pyroxene and sodic plagioclase feldspar that were mechanically derived and underwent minimal chemical change before deposition, and are otherwise either absent or present in very small amounts in the rest of the section. Flood basalts and rhyolite of Deccan origin are dominant at Pavagarh hill. The Godhra granite lies close to and nearby to the adjoining part of Pavagarh hill, which are underlain by the Precambrian basement made up of granites, gneisses, and quartzites (Sheth and Melluso, 2008). Pavagarh Hill has a wide variety of rock types, including picrite, sub-alkali basalt, and dacite to rhyolite, as well as a sizable amount of plagioclase and pyroxene phenocrysts (Sheth and Melluso, 2008). Both plagioclase and pyroxene are said to be weathering-prone (Goldich, 1938), yet their presence in the sediments suggests that weathering had not yet altered them prior to deposition. This has a significant effect on the geochemistry of the sediments, which show a positive correlation between mobile (Na_2O, MgO) and immobile elements (Al_2O_3 and Fe_2O_3) (Fig. 7, Table 3). This finding is further supported by the log (Na_2O/K_2O) versus log (SiO_2/Al_2O_3) plot (Fig. 9a; Pettijohn et al., 1972), where a substantial number of samples fall in the sub-litharenite group or are close to this field, indicating the existence of lithic components in the bulk sediment.

The presence of lithic components in the sediments indicates minimal chemical alteration. The presence of very fresh mineral grains of pyroxene and plagioclase also corroborates that the rocks of the upland catchment must have been exposed very recently or the conditions at the depositional site were such that there was no alteration before the sediments were deposited. The sediment samples were plotted on A–CN–K triangular plots to determine chemical maturity (Fig. 9c), and the samples plotted close to the post-Archean Australian Shale standard (PAAS). PAAS refers to the upper continental crust composition, and is used as a standard for comparing geochemical data. The CIA values in the examined sediments range from 55–74 (average = 69), which indicates that the sediment profile underwent mild weathering that was probably influenced by secondary calcrete formation. The ICV values, which represent chemically immature sediment from the first cycle of the sedimentary process, range from 0.99–2.6 (average = 1.50). High average ICV values (~1) are a result of sediments deposited in a tectonically active continental margin during the first cycle, and ICV values of <1 show highly mature sediments (i.e., enriched in resistant minerals) deposited after significant sediment recycling. Using the methods of Lee (2002), the CIA versus ICV plot (Fig. 9b) indicates that the sub-alkali and the picritic basalts are the major contributors of sediments in the Pratappura profile.

The REE abundance and chondrite normalized diagrams (Fig. 10a) show almost identical patterns, with a higher concentration of light REE (LREE) rather than heavy REE (HREE) with a negative Eu anomaly similar to that of the upper continental crust (UCC; McLennan, 2001), which indicates that the

https://doi.org/10.1017/qua.2022.39 Published online by Cambridge University Press

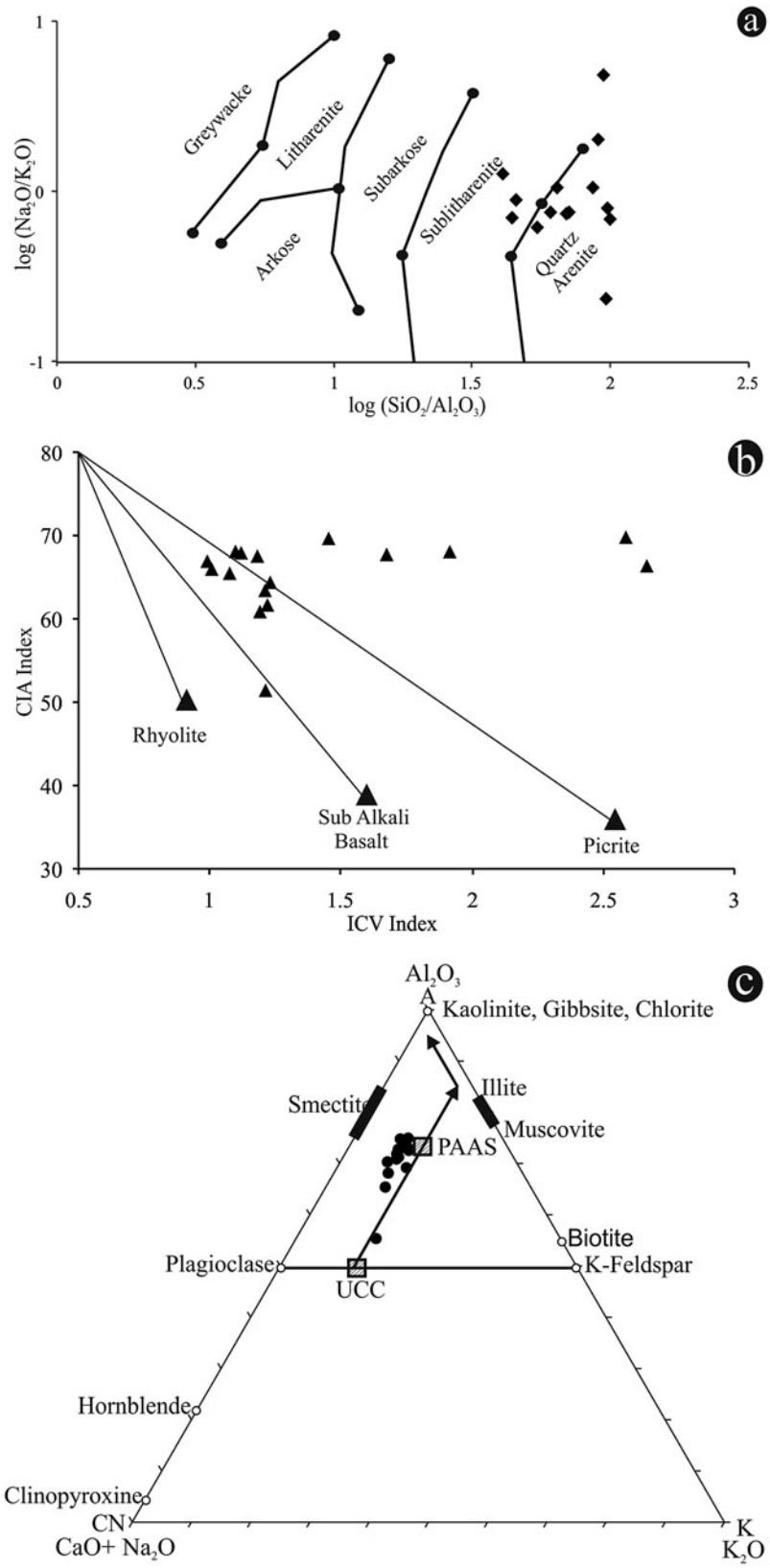

Figure 9. Plots of sediment chemical compositions of samples (see Table 2) from the Pratappura section. (a) Plot of log Na_2O/K_2O versus log SiO_2/Al_2O_3 (after Pettijohn et al., 1972); note the clustering of the samples between sublitharenite and quartz arenite fields, suggesting the presence of lithic components in the bulk sediment. (b) Plot of chemical index of alteration (CIA) versus index of chemical variability (ICV); note that samples cluster mainly between subalkali basalt and picrite, indicating the dominance of the mafic component. (c) A–CN–K plot; note that the Pratappura samples plot below the post-Archean Australian Shale (PAAS) standard, indicating moderate weathering in the presence of mafic components.

https://doi.org/10.1017/qua.2022.39 Published online by Cambridge University Press

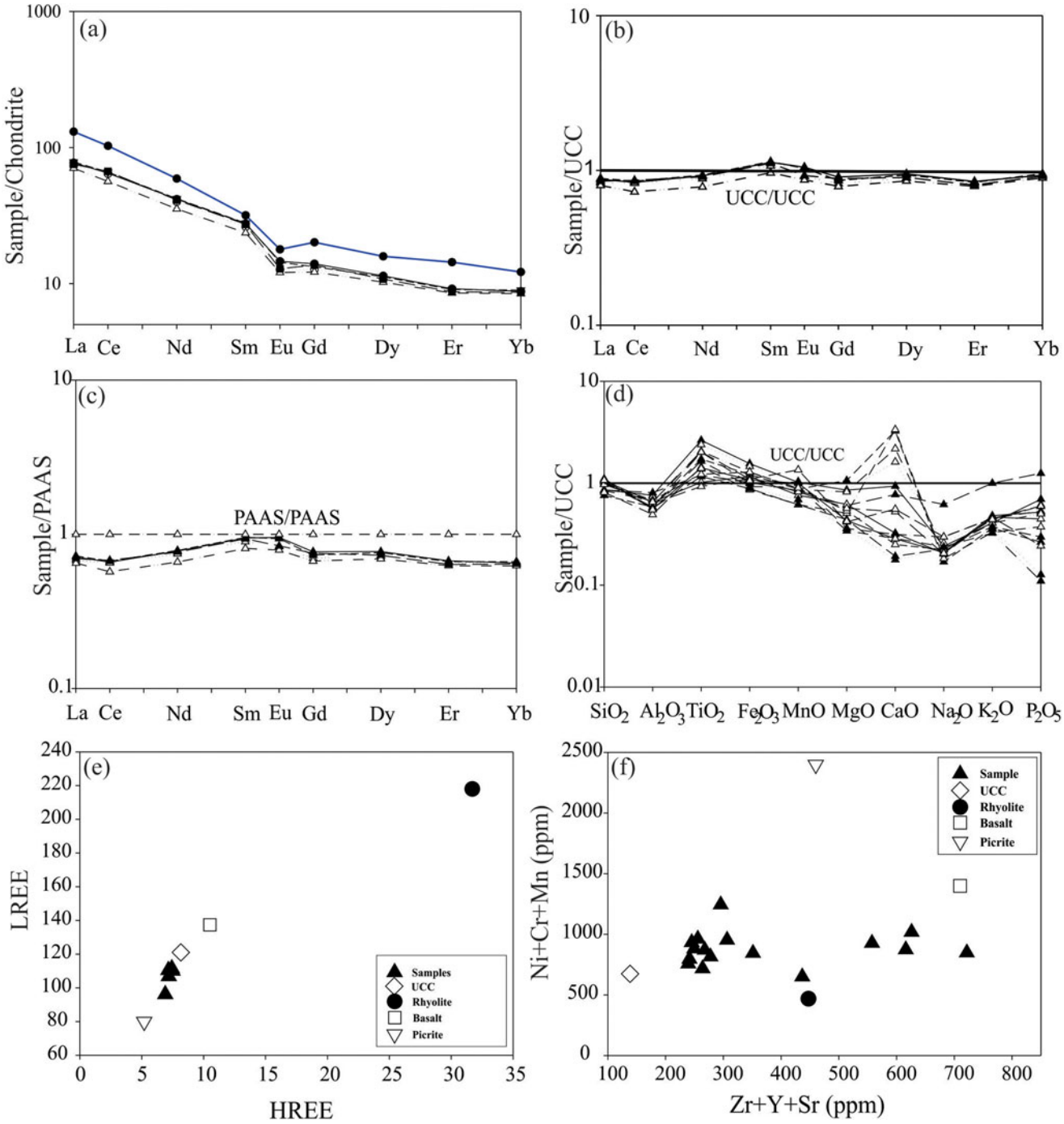

Figure 10. Rare earth element (REE) patterns for selected Pratappura samples (see Table 2). (a) Chondrite-normalized REE plots showing an upper continental crust (UCC) pattern; (b) UCC-normalized REE patterns with characteristic depleted light REE (LREE) and heavy REE (HREE) with enriched middle REE (MREE); (c) Post-Archean Australian Shale (PAAS)-normalized REE patterns showing less fractionated character and depleted REE values; (d) UCC-normalized multielement data shows enrichment of TiO_2 and Fe_2O_3 than UCC; (e) in both LREE versus HREE and (f) Ni+Cr+Mn versus Zr+Y+Sr scatter plots, all samples cluster close to UCC and picrite, indicating a mafic source. Chondrite data from McDonough and Sun (1995), UCC from Rudnick and Gao (2003), and PAAS from Taylor and McLennan (1985).

sediment samples are well homogenized. Similar to the LREE-deficient patterns, where the La/Yb <1, these sediments likely came from a mafic source. Depletion can be seen in the UCC- and PAAS-normalized REE patterns, although a hump in the middle REE could be due to pyroxene/amphiboles (Fig. 10b, c). The enrichment of TiO_2 and Fe_2O_3 compared to UCC can also be seen in the multi-element plot (Fig. 10d). Additionally, all samples plot close to UCC and between picrite and sub-alkali basalt in the LREE versus HREE plot (Fig. 10e). In contrast, the samples plot between the fields of basalt and rhyolite in Ni+Cr+Mn versus Zr+Y+Sr (compatible versus incompatible elements; Fig. 10f). These diagrams imply that

https://doi.org/10.1017/qua.2022.39 Published online by Cambridge University Press

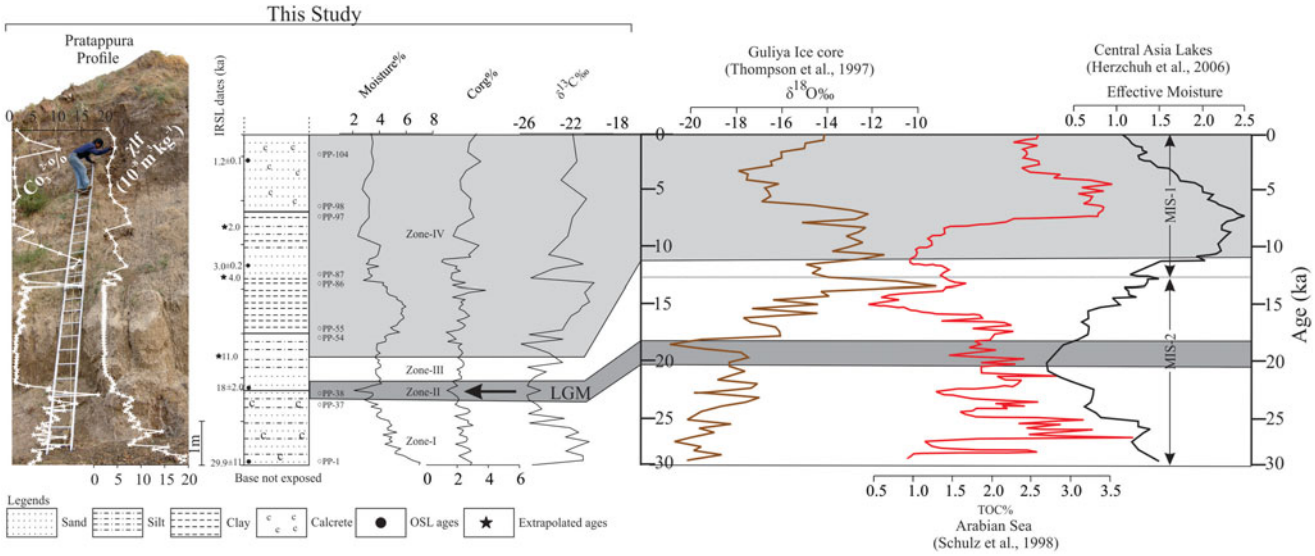

Figure 11. Photograph and graphic measured section of the lithostratigraphy of the Pratappura profile from the Dhadhar River (mainland Gujarat, western India), variation of percentages of moisture, C_{org}, CO_3^{-2}, and magnetic susceptibility (χ_{lf}), and $\delta^{13}C$ plotted with positions in the Pratappura profile. The major climatic records derived from this profile were compared with oxygen isotopic data from the Guliya ice core (Thompson et al., 1997). Enriched values of $\delta^{18}O$ indicate periods of strengthened Indian summer monsoon (ISM) and lower values indicate a weaker ISM (dry phase). Total organic carbon (%TOC) is a proxy for productivity, and therefore is an indicator of monsoon-induced upwelling from the northern Arabian Sea (Schulz et al., 1998). Central Asian lake records (Herzchuh, 2006) indicate wet conditions during the middle and late Marine Isotope Stage 3 (MIS-3) and dry conditions during the Last Glacial Maximum (LGM).

the samples exhibit a bias towards a source that is dominated by basalt. However, there is also an indication of a felsic component.

Paleoclimatic inferences

The Pratappura profile was divided into five climatic zones in chronological sequence for accurate assessment and sequential changes in the major proxy metrics including grain size, $\delta^{13}C$, elemental analysis, magnetic susceptibility (χ_{lf}), loss-on-ignition (LOI), and phytoliths (Figs. 4, 8). Additionally, the four OSL dates presented with depth (Fig. 2) restrict us to suggest only climatic events of the past ca. 30 ka. To overcome this, specific observations are discussed using extrapolated ages determined by sedimentation rate.

A steadily increasing trend in the sand and the carbonate carbon fraction is seen in zone-I (29.9–18 ka). In contrast, moisture content, % C_{org}, and magnetic susceptibility (χ_{lf}) all trend downward. An increase in CO_3^{-2} fraction indicates evaporative conditions that favored the development of secondary calcrete (Khadkikar et al., 2000). Similarly, the decline in χ_{lf}, Al_2O_3, Fe_2O_3, TiO_2, and CIA is also thought to be a consequence of hydrological conditions gradually diminishing with a decrease in sediment supply and less chemical weathering in the catchment region (Evans and Heller, 1994; Figs. 4, 6). The region's semiarid climate is also indicated by a change in clay mineralogy from smectite–kaolinite to mainly smectite (Jain and Tandon, 2003; Fig. 5b). It is important to note numerous researchers in the Sabarmati and the Mahi River valleys reported regional flood plain aggradation and pedogenesis activities during MIS-3 (Juyal et. al., 2006; Thokchom et al., 2017). The central Thar Desert region (Andrews et al., 1998; Jain and Tandon, 2003), the northwestern Deccan highland region (Kale and Rajaguru, 1987), the southern Ganga (Singh et al., 1999), and the Sabarmati River alluvial plains, and the north Gujarat area (Srivastava et al., 2001) all reported similar records. Juyal et al. (2006) hypothesized that the climate during floodplain aggradation in MIS-3 was likely comparable to or wetter than it is today based on the regional nature of the aggradation. However, as MIS-2 (29–18 ka) began, hydrological conditions gradually deteriorated as seen in the declining moisture content of the sediments (Fig. 4). Additionally, this time period shows fluvial aggradation in the rivers of western India as a result of lower Indian summer monsoon (ISM) intensity. Interestingly, this was also the time when increased aridity started in the region (Juyal et al., 2006). According to Bhattacharya et al. (2017, and references therein), the Banas River basin experienced a relatively enhanced ISM with fluctuations during the early MIS-2 (25 ka). Similar conclusions can be derived for the lower part of the alluvial sequence in the Saraswati River (dated to 32 ka).

Additionally the lower intensity of ISM and the deterioration of moisture conditions after 25.5 ka and the moisture minimum seen in central Asia between 21.3 ka and 19.8 ka (Herzchuh, 2006). Similar conclusions were made from the Guliya ice core records by Thompson et al. (1997), who found that high $\delta^{18}O$ values suggested an enhanced summer monsoon, and lower values indicated a reduction in ISM. A stronger ISM during the MIS-2 is also indicated by the Arabian Sea records (Schulz et al., 1998) and 75 paleoclimatic records from central Asian lakes (Herzchuh, 2006; Fig. 11).

Zone-II (18–11 ka), which corresponds to the Last Glacial Maximum (LGM), is composed of an increasing sand fraction, a lower CIA, Al_2O_3, and high CaO values, and mostly stable χ_{lf} and C_{org} values, which indicate that moisture conditions weakened, and an increase in aridity occurred at this time (Figs. 4 and 6). It is clear that moderately weathered sand dated between ca. 27–20 ka in the Mahi River valley and along the southern edge of Thar Desert indicates poor hydrological conditions corresponding to an increase in aridity during the LGM. According

https://doi.org/10.1017/qua.2022.39 Published online by Cambridge University Press

to Guliya ice core data in Thompson et al. (1997) and records from the Arabian Sea in Schultz et al. (1998), this LGM episode occurred ca. 20 ka.

The phytoliths and χ_{lf} in zone-III (11–4 ka) show a noticeable change, with increasing silt and clay percentage primarily derived from the Pavagarh Hills of the Deccan volcanic suite, yet increased moisture content and Al_2O_3 and $\delta^{13}C$ values indicate improved climatic conditions (Fig. 4). It is fascinating to see that this area now had more moisture and charcoal, and that the phytoliths display signs of burning. This suggests that the climate improved slightly becoming wetter, and the material that was needed to form overbank deposits along with charcoal must have been brought by intermittent heavy rains. A minor improvement in climatic conditions is indicated by a slight rise in immobile elements and a shift in the proportion of clay that is dominated by smectite to more clay minerals and a mixed signal from C_3 and C_4 grasses. ISM intensification during the early Holocene between 11 ka and 9.5 ka from central India was also observed by Kumar et al. (2019). Overall conditions, however, continued to be more favorable for winter grasses, demonstrating that regional hydrological conditions were controlled by winter precipitation (Raj et al., 2003; Prasad et al., 2007, 2014; Raj, 2007).

Metrics for zone-IV (4–2 ka; Figs. 4 and 6) vary as does the lithology, which consists of alternating black and brown sandy concretized beds. Although phytolith morphotypes indicate a moderately wet pulse near the end of this zone, the fluctuations seen in χ_{lf}, % C_{org} and CO_3^{-2}, and $\delta^{13}C$ values also imply an increase in moisture content. The beginning of the channel activity (river flow) coincides with the ISM's late Holocene intensification, which appears to have continued sporadically in mainland Gujarat until ca. 2 ka. The Banas River's 1.5 m-deep channel sand was dated to 1 ± 0.1 ka, and paleoflood sediments also gave an identical age that roughly coincides with the Medieval Warm Period (MWP; Bhattacharya et al., 2017). Similar evidence of large floods associated with the MWP is reported from the Luni River (Thar Desert; Kale et al., 2000) and the Sabarmati River (Sridhar et al., 2014). In zone-V (2 ka to present), there were very negligible changes in the proxies. The phytolith morphotypes (Fig. 8) towards the top of this zone indicate a change in climate that indicates the advancement of the summer monsoon. Overall, based on a robust laboratory dataset corroborating prior field-based results, we have a generalized idea of what the paleoclimates of this area have been from ca. 30 ka to present. The Pratappura profile sediment sequence is a viable site for determining paleoclimate in this area of India, and multiproxy research helps us to describe the various climatic events of the past ca. 30 ka as outlined above.

CONCLUSIONS

We used a multiproxy approach to analyze the sediments from the Pratappura profile using sedimentological and geochemical characteristics, χ_{lf}, $\delta^{13}C$, and phytoliths to determine weathering history, sediment provenance, and to derive a paleoclimatic history of this region of western India. Analyses of the Pratappura profile sediments using multiple proxies show a complex climate and sedimentological history. Silty-sand and sandy-silt facies cluster in the quartz arenite and sub-litharenite categories in a log Na_2O/K_2O versus log SiO_2/Al_2O_3 plot, indicating low to moderate weathering. The CIA ranges from 55–74 and was plotted against the calculated ICV of 1.50, and samples clustered mainly between subalkali basalt and picrite, indicating the dominance of a mafic component in the sediments. Identical chondrite normalized REE patterns suggest that sediments are well-homogenized, and depleted chondrite normalized light REE ($La/Yb < 1$) values also suggest the prevalence of a mafic source for sediments in the catchment.

OSL was done for four samples and provided extrapolated dates for the section, and multiproxy data including moisture, χ_{lf}, % C_{org} and % CO_3^{-2}, $\delta^{13}C$, and phytolith analyses indicate that the section could be divided into five paleoclimate zones. The climate in the region changed from warm and humid to semiarid conditions between ca. 29 ka to 18 ka, but the LGM period marks the beginning of aridity. The period between ca. 18 ka and ca. 11 ka indicates less available moisture and a commensurate rise in aridity. When monsoon conditions appear in the early Holocene (ca. 11 ka to 4 ka), the climate starts to show an increase in moisture, but a wet phase is only noted between 4 ka and 2 ka. Between 2 ka and present, no discernible change in climate was noted; the regional climate was semiarid through this time.

Acknowledgments. We thank the director at BSIP Lucknow for providing the necessary help and support to carry out the work. We also thank directors at WIHG (Dehradun) and IITM (Pune) for providing analytical facilities. We thank five anonymous reviewers for their valuable comments, thus helping to improve the quality of the article. The current work is a part of the project (SR/S4/ES 21/Baroda Window/P1) of the Shallow Subsurface Study (SSS) program of the Department of Science and Technology (DST), New Delhi. The authors declare that they have no known competing financial interests or personal relationships that could have appeared to influence the work reported in this paper.

Supplementary Material. The supplementary material for this article can be found at https://doi.org/10.1017/qua.2022.39

REFERENCES

Andrews, J.E., Singhvi, A.K., Kailath, J.A., Kuhn, R., Dennis, P.F., Tandon, S.K., Dhir, R.P., 1998. Do stable isotope data from calcrete record Late Pleistocene monsoonal climate variation in the Thar Desert of India? *Quaternary Research* **50**, 240–251.

Armstrong-Altrin, J.S., 2015. Evaluation of two multidimensional discrimination diagrams from beach and deep-sea sediments from the Gulf of Mexico and their application to Precambrian clastic sedimentary rocks. *International Geology Review* **57**, 1446–1461.

Bengtsson, L., Enell, M., 1986. Chemical analysis. In: Berglund, B.E. (Ed.), *Handbook of Holocene Palaeoecology and Palaeohydrology*. John Wiley & Sons, Chichester, pp. 423–451.

Bhandari, S., Maurya, D.M., Chamyal, L.S., 2005. Late Pleistocene alluvial plain sedimentation in Lower Narmada Valley, Western India: palaeoenvironmental implications. *Journal of Asian Earth Sciences* **24**, 433–444.

Bhattacharya, F., Shukla, A.D., Patel, R.C., Rastogi, B.K., Juyal, N., 2017. Sedimentology, geochemistry and OSL dating of the alluvial succession in the northern Gujarat alluvial plain (western India)–A record to evaluate the sensitivity of a semiarid fluvial system to the climatic and tectonic forcing since the late Marine Isotopic Stage 3. *Geomorphology* **297**, 1–19.

Biswas, S.K., 1987. Regional tectonic framework, structure and evolution of the western marginal basins of India. *Tectonophysics* **135**, 307–327.

Bridge, J.S., 1985. Paleochannel patterns inferred from alluvial deposits; a critical evaluation. *Journal of Sedimentary Petrology* **55**, 579–589.

Bristow, C., 1996. Reconstructing fluvial channel morphology from sedimentary sequences. In: Carling, P.A., Dawson, M.R. (Eds.), *Advances in Fluvial Dynamics and Stratigraphy*. Wiley, New York, pp. 351–371.

Cant, D.J., Walker, R.G., 1978. Fluvial processes and facies sequences in the sandy braided South Saskatchewan River, Canada. *Sedimentology* **25**, 625–648.

Coplen, T.B., 1994. Reporting of stable hydrogen, carbon, and oxygen isotopic abundances. *Pure and Applied Chemistry* **66**, 273–276.

Cox, R., Lowe, D.R., Cullers, R.L., 1995. The influence of sediment recycling and basement composition on evolution of mudrock chemistry in the

southwestern United States. *Geochimica et Cosmochimica Acta* **9**, 2919–2940

Day, P.R., 1965. Particle fractionation and particle-size analysis. In: Black, C.A. (Ed.), *Methods of Soil Analysis. Part I. Agronomy Monographs* 9.1, American Society of Agronomy, Madison, Wisconsin, pp. 545–577.

Dean, W.E., 1974. Determination of carbonate and organic matter in calcareous sediments and sedimentary rocks by loss on ignition; comparison with other methods. *Journal of Sedimentary Petrology* **44**, 242–248.

ESRI, 2011. ArcGIS Desktop: Release 10. Redlands, CA: Environmental Systems Research Institute.

Evans, M.E., Heller, F., 1994. Magnetic enhancement and palaeoclimate. Study of a loess/palaeosol couplet across the Loess Plateau of China. *Geophysical Journal International* **117**, 257–264.

Fredlund, G.G., Tieszen, L.T., 1994. Modern phytolith assemblages from the North American Great Plains. *Journal of Biogeography* **21**, 321–335.

Galbraith, R.F., Roberts, R.G., Laslett, G.M., Yoshida, H., Olley, J.M., 1999. Optical dating of single and multiple grains of quartz from Jinmium rock shelter, Northern Australia: Part I, experimental design and statistical models. *Archaeometry* **41**, 339–364.

Gates-Rector, S., Blanton, T.N., 2019. The Powder Diffraction File: A quality materials characterization database. *Powder Diffraction* **34**, 352–360.

Goldich, S.S., 1938. A study on rock weathering. *Journal of Geology* **46**, 17–58.

Herzchuh, U., 2006. Paleo-moisture evolution in monsoonal central Asia during the last 50,000 years. *Quaternary Science Review* **25**, 163–178.

Jackson, M.L., 1956. *Soil Chemical Analysis-Advanced Course*. Published by the author, College of Agriculture, Department of Soils, University of Wisconsin, Madison, USA.

Jain, M., Tandon, S.K., 2003. Quaternary alluvial stratigraphy and palaeoclimactic reconstruction at the Thar margin. *Current Science* **84**, 1048–1055.

Jain, M., Tandon, S.K., Bhatt, S.C., 2004. Late Quaternary stratigraphic development in the lower Luni, Mahi and Sabarmati river basins, western India. *Journal of Earth System Science* **113**, 453–471.

Juyal, N., Chamyal, L.S., Bhandari, S., Bhushan, R., Singhvi, A.K., 2006. Continental record of the southwest monsoon during the last 130 ka: evidence from the southern margin of the Thar Desert, India. *Quaternary Science Reviews* **25**, 2632–2650.

Juyal, N., Chamyal, L.S., Bhandari, S., Maurya, D.M., Singhvi, A.K., 2004. Environmental changes during Late Pleistocene in the Orsang River basin, Western India. *Journal of the Geological Society of India* **64**, 471–479.

Juyal, N., Kar, A., Rajaguru, S.N., Singhvi, A.K., 2003. Luminescence chronology of aeolian deposition during the Late Quaternary on the southern margin of Thar Desert, India. *Quaternary International* **104**, 87–98.

Juyal, N., Raj, R., Maurya, D.M., Chamyal, L.S., and Singhvi, A.K., 2000. Chronology of Late Pleistocene environmental changes in the lower Mahi basin, western India. *Journal of Quaternary Science* **15**, 501–508.

Kale, V.S., Rajaguru, S.N., 1987. Late Quaternary alluvial history of the northwestern Deccan upland region. *Nature* **325**, 612–614.

Kale, V.S., Singhvi, A.K., Mishra, P.K., Banerjee, D., 2000. Sedimentary records and luminescence chronology of Late Holocene palaeofloods in the Luni River, Thar Desert, northwest India. *Catena* **40**, 337–358.

Khadkikar, A.S., Chamyal, L.S., Ramesh, R., 2000. The character and genesis of calcrete in late Quaternary alluvial deposits, Gujarat, western India, and its bearing on the interpretation of ancient climates. *Palaeogeography, Palaeoclimatology, Palaeoecology* **162**, 239–261.

Khanna, P.P., Saini, N.K., Mukherjee, P.K., Purohit, K.K., 2009. An appraisal of ICP-MS technique for determination of REEs: long term QC assessment of silicate rock analysis. *Himalayan Geology* **30** (1), 95–99.

Knox, J.C., 1995. Fluvial systems since 20,000 years BP. In: Gregory, K.J., Starkel, L., Baker, V.R. (Eds.), *Global Continental Palaeohydrology*. Wiley, New York, pp. 87–108.

Kumar, K., Agrawal, S., Sharma, A., Pandey, S., 2019. Indian summer monsoon variability and vegetation changes in the core monsoon zone, India, during the Holocene: A multiproxy study. *The Holocene* **29**, 110–119.

Kunze, G.W., 1965. Pretreatment for mineralogical analysis. In: Black, C.A. (Ed.), *Methods of Soil Analysis. Part I. Agronomy Monographs* 9.1, American Society of Agronomy, Madison, Wisconsin, pp. 568–577.

Laskar, A.H., Sharma, N., Ramesh, R., Jani, R.A., Yadava, M.G., 2010. Paleoclimate and paleovegetation of Lower Narmada Basin, Gujarat, Western India, inferred from stable carbon and oxygen isotopes. *Quaternary International* **227**, 183–189.

Lee, Y., 2002. Provenance derived from the geochemistry of late Paleozoic–early Mesozoic mudrocks of the Pyeongan Supergroup, Korea. *Sedimentary Geology* **149**, 219–235.

Maher, B.A., Thompson, R., 1992. Paleoclimatic significance of the mineral magnetic record of the Chinese Loess and paleosols. *Quaternary Research* **37**, 155–170.

Maurya, D.M., Chamyal, L.S., Merh, S.S., 1995. Tectonic evolution of the Central Gujarat plain, western India. *Current Science* **69**, 610–613.

Maurya, D.M., Malik, J.N., Raj, R., Chamyal, L.S., 1997. Holocene valley-fill terraces in the Lower Mahi valley, Gujarat. *Current Science* **73**, 539–542.

Maurya, D.M., Raj, R., Chamyal, L.S., 2000. History of tectonic evolution of Gujarat alluvial plains, western India during Quaternary: a review. *Journal of the Geological Society of India* **55**, 343–366.

McDonough, W.F., Sun, S.S., 1995. The composition of the earth. *Chemical Geology* **120**, 223–253.

McLennan, S.M., 1993. Weathering and global denudation. *The Journal of Geology* **101**, 295–303.

McLennan, S.M., 2001. Relationships between the trace element composition of sedimentary rocks and upper continental crust. *Geochemistry Geophysics Geosystems* **2**, 1021.

Merh, S.S., Chamyal, L.S., 1997. The Quaternary geology of Gujarat Alluvial Plains. *Proceedings of the Indian National Science Academy* **63**, 1–98.

Moore, I.D., Grayson, R.B., Ladson, A.R., 1991. Digital terrain modelling: a review of hydrological, geomorphological, and biological applications. *Hydrological Processes* **5**, 3–30.

Mulholland, S.C., Rapp, G., Jr., 1992. A morphological classification of grass silica-bodies. In: Mulholland, S.C., Rapp, G., Jr. (Eds), *Phytolith Systematics. Emerging Issues. Advances in Archaeological and Museum Science, Vol.* 1, Springer, Boston, pp. 65–90.

Murray, A.S., Wintle, A.G., 2000. Luminescence dating of quartz using an improved single-aliquot regenerative-dose protocol. *Radiation Measurements* **32**, 57–73.

Nesbitt, H.W., Young, G.M., 1989. Formation and diagenesis of weathering profiles. *The Journal of Geology* **97**, 129–147.

Pettijohn, F.J., Potter, P.E., Siever, R., 1972. *Sand and Sandstone*. Springer-Verlag, New York.

Phartiyal, B., Srivastava, P., Sharma, A., 2009. Tectono-climatic signatures during late Quaternary Period from Upper Spiti Valley, NW Himalaya, India. *Himalayan Geology* **30**(2), 164–174.

Potter, P.E., Pettijohn, F.J., 1963. *Paleocurrents and Basin Analysis*. Academic Press, New York, 330 pp.

Prasad, S., Anoop, A., Riedel, N., Sarkar, S., Menzel, P., Basavaiah, N., Krishnan, R., *et al.*, 2014. Prolonged monsoon droughts and links to Indo-Pacific warm pool: A Holocene record from Lonar Lake, central India. *Earth and Planetary Science Letters* **391**, 171–182.

Prasad, V., Phartiyal, B., Sharma, A., 2007. Evidence of enhanced winter precipitation and the prevalence of a cool and dry climate during the mid to late Holocene in mainland Gujarat, India. *The Holocene* **17**, 889–896.

Prescott, J.R., Stephan, L.G., 1982. Contribution of cosmic radiation to the environmental dose for thermoluminescent dating: Latitude, altitude and depth dependences. *PACT: Journal of the European Study Group on Physical, Chemical and Mathematical Techniques Applied to Archaeology* **6**, 17–25.

Raj, R., 2007. Late Pleistocene fluvial sedimentary facies, the Dhadhar River basin, Western India. *Quaternary International* **159**, 93–101.

Raj, R., Maurya, D.M., Chamyal, L.S., 1998. Late Quaternary sea level changes in Western India: Evidence from lower Mahi valley. *Current Science* **74**, 910–914.

Raj, R., Mulchandani, N., Bhandari, S., Maurya, D.M., Chamyal, L.S., 2003. Evidence of a Mid–Late Holocene seismic event from Dhadhar river basin, Gujarat alluvial plain, western India. *Current Science* **85**, 812–815.

https://doi.org/10.1017/qua.2022.39 Published online by Cambridge University Press

Reddy, R.K.T., 1991. Digital analysis of lineaments—a test study on South India. *Computers & Geosciences* **17**, 549–559.

Rudnick, R.L., Gao, S., 2003. *Composition of the continental crust*. In: Holland, H.D., Turekian, K.K. (Eds.), *Treatise on Geochemistry*, Pergamon Press, Oxford, England. pp. 1–64.

Saini, N.K., Mukherjee, P.K., Rathi, M.S., Khanna, P.P., 2000. Evaluation of energy-dispersive X-ray fluorescence spectrometry in the rapid analysis of silicate rocks using pressed powder pellets. *X-ray Spectrometry* **29**, 166–72.

Sanderson, D., Peacock, D., 2020. Making rose diagrams fit-for-purpose. *Earth-Science Reviews* **201**, 103055. https://doi.org/10.1016/j.earscirev.2019.103055.

Sangode, S.J., Mazari, R.K., 2007. Mineral magnetic response to climate variability in the high altitude Kioto palaeolake, Spiti Valley, Northwestern Himalaya. *Himalayan Geology* **28**(2), 1–9.

Schulz, H., von Rad, U., Erlenkeuser, H., 1998. Correlation between Arabian Sea and Greenland climate oscillations of the past 110,000 years. *Nature* **393**, 54–57.

Schumm, S.A., 1993. River response to baselevel change: implications for sequence stratigraphy. *The Journal of Geology* **101**, 279–294.

Shapiro, L., Brannock, W.W., 1962. Rapid analysis of silicate, carbonate and phosphate rocks. *United States Geological Survey Bulletin* 1144-A, A1–A56.

Sharma, A., Sensarma, S., Kumar, K., Khanna, P.P., Saini, N. K., 2013. Mineralogy and geochemistry of the Mahi River sediments in tectonically active western India: Implications for Deccan large igneous province source, weathering and mobility of elements in a semi-arid climate. *Geochimica et Cosmochimica Acta* **104**, 63–83

Sheth, H., Melluso, L., 2008. The Mount Pavagadh volcanic suite, Deccan Traps: Geochemical stratigraphy and magmatic evolution. *Journal of Asian Earth Sciences* **32**, 5–21.

Singh, I.B., Sharma, S., Sharma, M., Srivastava, P., Rajagopalan, G., 1999. Evidence of human occupation and humid climate of 30 ka in the alluvium of southern Ganga Plain. *Current Science* **76**, 1022–1026.

Singh, V., Prasad, V., Chakraborty, S., 2007. Phytoliths as indicators of monsoonal variability during mid-late Holocene in mainland Gujarat, western India. *Current Science* **92**, 1754–1759.

Sridhar, A., Chamyal, L.S., Patel, M., 2014. Palaeoflood record of high-magnitude events during historical time in the Sabarmati River, Gujarat. *Current Science* **107**, 675–679.

Srivastava, P., Juyal, N., Singhvi, A.K., Wasson, R.J., Bateman, D., 2001. Luminescence chronology of river adjustment and incision of Quaternary sediments in the alluvial plain of Sabarmati River, north Gujarat, India. *Geomorphology* **36**, 217–229.

Stork, A.L., Smith, D.K., Gill, J.B., 1987. Evaluation of geochemical reference standards by X-ray fluorescence analysis. *Geostandards Newsletter* **11**, 107–113.

Tandon, S.K., Sareen, B.K., Someshwar Rao, M., Singhvi, A.K., 1997. Aggradation history and luminescence chronology of Late Quaternary semi-arid sequence of the Sabarmati basin, Gujarat, Western India. *Palaeogeography Palaeoclimatology, Palaeoecology* **128**, 339–357.

Tanner, C.B., Jackson, M.L., 1948. Nomographs of sedimentation times for soil particles under gravity or centrifugal acceleration. *Proceedings of the Soil Science Society of America* **12**, 60–65.

Taylor, S.R., McLennan, S.M., 1985. *The Continental Crust: its Composition and Evolution*. Blackwell Scientific, Malden, Massachusetts, 312 pp.

Thokchom, S., Bhattacharya, F., Prasad, A.D., Dogra, N.N., Rastogi, B.K., 2017. Paleoenvironmental implications and drainage adjustment in the middle reaches of the Sabarmati River, Gujarat: implications towards hydrological variability. *Quaternary International* **454**, 1–14.

Thompson, L.G., Yao, T., Davis, M.E., Henderson, K.A., Mosley-Thompson, E., Lin, P.N., Beer, J., Synal, H.-A., Cole-Dai, J., Bolzan, J.F., 1997. Tropical climate instability: the Last Glacial Cycle from a Qinghai-Tibetan ice core. *Science* **276**, 1821–1825.

Twiss, P.C., Suess, E., Smith, R.M., 1969. Morphological classification of grass phytoliths. *Proceedings of the Soil Science Society of America* **33**, 109–115.

Williamson, D., Jackson, M.J., Banerjee, S.K., Marvin, J., Merdaci, O., Thouveny, N., Decobert, M., Gibert-Massault, E., Massault, M., Mazaudier, D., Taieb, M., 1999. Magnetic signatures of hydrological change in a tropical maar-lake (Lake Massoko, Tanzania): preliminary results. *Physics and Chemistry of the Earth, Part A: Solid Earth and Geodesy* **24**, 799–803.

https://doi.org/10.1017/qua.2022.39 Published online by Cambridge University Press